NASA TECHNICAL
MEMORANDUM

NASA TM X-53501

1965

NASA TM X-53501

RESEARCH ACHIEVEMENTS REVIEW SERIES NO.12

RESEARCH AND DEVELOPMENT OPERATIONS
GEORGE C. MARSHALL SPACE FLIGHT CENTER
HUNTSVILLE, ALABAMA

GEORGE C. MARSHALL SPACE FLIGHT CENTER

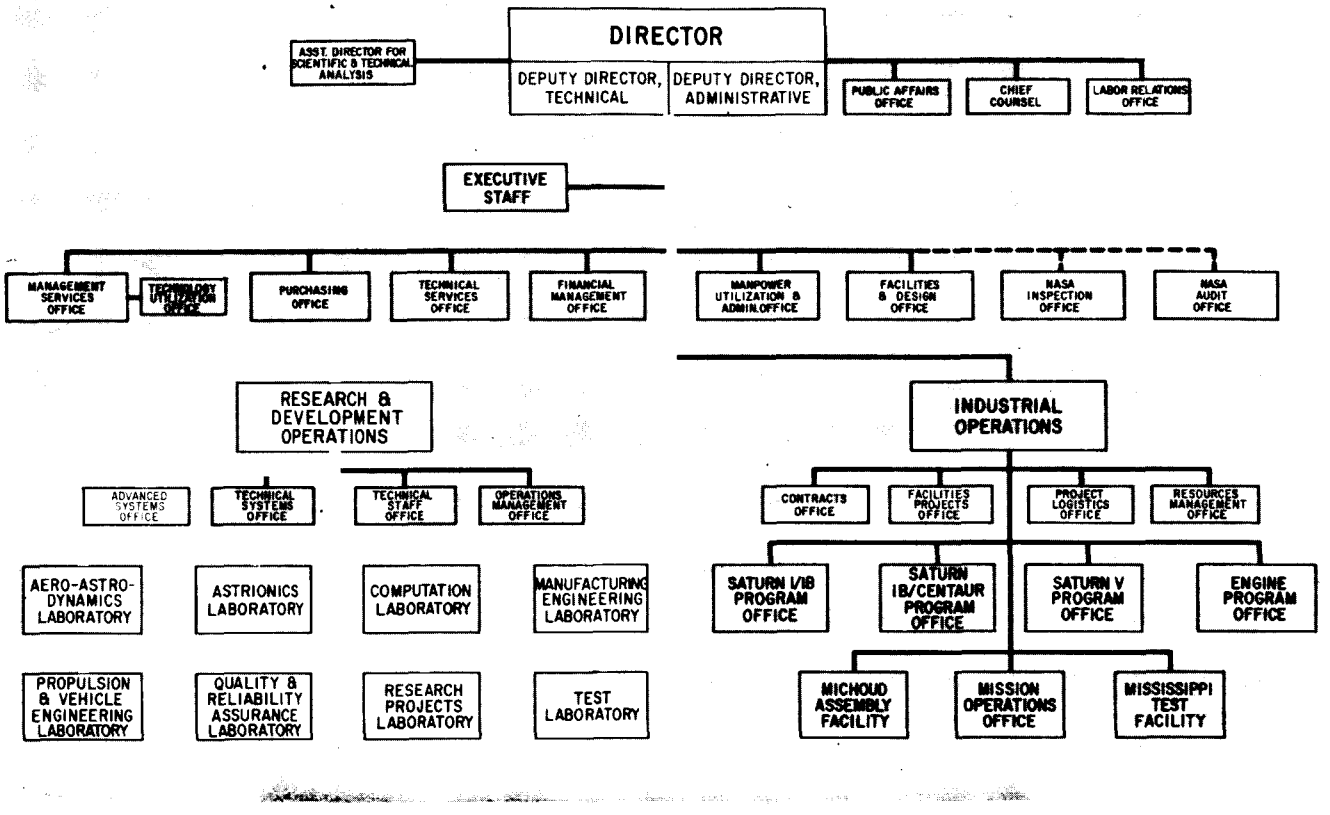

RESEARCH ACHIEVEMENTS REVIEW SERIES INCLUDES THE FOLLOWING FIELDS OF RESEARCH

1. RADIATION PHYSICS
2. THERMOPHYSICS
3. CHEMICAL PROPULSION
4. CRYOGENIC TECHNOLOGY
5. ELECTRONICS
6. CONTROL SYSTEMS
7. MATERIALS
8. MANUFACTURING
9. GROUND TESTING
10. QUALITY ASSURANCE AND CHECKOUT
11. TERRESTRIAL AND SPACE ENVIRONMENT
12. AERODYNAMICS
13. INSTRUMENTATION
14. POWER SYSTEMS
15. GUIDANCE CONCEPTS
16. ASTRODYNAMICS
17. ADVANCED TRACKING SYSTEMS
18. COMMUNICATION SYSTEMS
19. STRUCTURES
20. MATHEMATICS AND COMPUTATION
21. ADVANCED PROPULSION
22. LUNAR AND METEOROID PHYSICS

NASA TM X-53501

NATIONAL AERONAUTICS AND SPACE ADMINISTRATION
WASHINGTON, D. C.

AERODYNAMICS RESEARCH AT MSFC

RESEARCH ACHIEVEMENTS REVIEW SERIES NO. 12

RESEARCH AND DEVELOPMENT OPERATIONS
GEORGE C. MARSHALL SPACE FLIGHT CENTER
HUNTSVILLE, ALABAMA

1965

PREFACE

In 1955, the team which has become the Marshall Space Flight Center (MSFC) began to organize a research program within its various laboratories and offices. The purpose of the program was two-fold: first, to support existing development projects by research studies and second, to prepare future development projects by advancing the state of the art of rockets and space flight. Funding for this program came from the Army, Air Force, and Advanced Research Projects Agency. The effort during the first year was modest and involved relatively few tasks. The communication of results was, therefore, comparatively easy.

Today, more than ten years later, the two-fold purpose of MSFC's research program remains unchanged, although funding now comes from NASA Program Offices. The present yearly effort represents major amounts of money and hundreds of tasks. The greater portion of the money goes to industry and universities for research contracts. However, a substantial research effort is conducted in house at the Marshall Center by all of the laboratories. The communication of the results from this impressive research program has become a serious problem by virtue of its very voluminous technical and scientific content.

The Research Projects Laboratory, which is the group responsible for management of the consolidated research program for the Center, initiated a plan to give better visibility to the achievements of research at Marshall in a form that would be more readily usable by specialists, by systems engineers, and by NASA Program Offices for management purposes.

This plan has taken the form of frequent Research Achievements Reviews, with each review covering one or two fields of research. These verbal reviews are documented in the Research Achievements Review Series.

Ernst Stuhlinger
Director, Research Projects Laboratory

These papers presented September 16, 1965

CONTENTS. . .

Page

INTRODUCTION TO RESEARCH ACHIEVEMENTS REVIEW ON AERODYNAMICS RESEARCH

by Dr. E. D. Geissler 1

GENERAL REVIEW OF AERODYNAMICS RESEARCH

by Werner Dahm

Page

I. INTRODUCTION 2

II. SUBSONIC FLOW 2

III. JET IMPACT IN WATER 3

IV. BASE FLOW INVESTIGATION 4

V. EFFECT OF WALL-TO-TOTAL TEMPERATURE RATIO ON HYPERSONIC FLOW DETACHMENT 5

VI. VARIABLE POROSITY WALLS 6

VII. DYNAMIC BALANCE FOR SATURN FOREBODY 7

LIST OF ILLUSTRATIONS

Figure	Title	Page
1.	Pressure Distribution about a Jupiter Nose Cone	3
2.	Drag Coefficient of Cones of Different Apex as a Function of the Base Pressure Coefficient	3
3.	Penetration Depth of Sub and Supersonic Jets in Water	4
4.	Recirculation Zone Flow Field	5
5.	Two-Dimensional Base Flow	5
6.	Schlieren Pictures of the Model at T_w/T_o = 0.88 and 0.22	6
7.	The Effect of T_w/T_o on the Drag Coefficient	7
8.	Photograph of 20° Cone-Cylinder in Tunnel	8
9.	Sketch of Variable Porosity Concept	8
10.	Cone-Cylinder Pressure Distribution at M = 1.10 with a Fixed Tunnel Wall Porosity of 7.5 Percent with 60° Slanted Holes	8

Figure	Title	Page
11.	Cone-Cylinder Pressure Distribution at M = 1.10 with Variable Porosity Walls Set at 1.6 Percent with 60° Slanted Holes	8
12.	Sting, Mounted Dynamic Balance	8

UNSTEADY AERODYNAMICS

by M. F. Platzer

		Page
	SUMMARY	9
I.	INTRODUCTION	9
II.	PANEL FLUTTER	9
III.	AERODYNAMIC-DAMPING STUDIES	10
IV.	BUFFETING	11
V.	ENGINE-GENERATED NOISE	12
VI.	GROUND-WINDS PROBLEM	12
VII.	CONCLUSIONS	13
	REFERENCES	13

LIST OF ILLUSTRATIONS

Figure	Title	Page
1.	Regions of X-15 Research Aircraft Affected by Panel Flutter	10
2.	Variation of Panel-Response Envelope with Dynamic Pressure Obtained from Flight Measurements on an X-15 Side-Fairing Panel	10
3.	Effect of Mach Number on Fixed Axis Damping in Pitch Moment Coefficient for Convex and Concave Parabolic Ogive of Thickness Ratio 0.1	11
4.	Flow Field about Typical Saturn Series Vehicle	11
5.	Typical Fluctuating Pressure Environment for Vehicle Interstage Type Geometries	11
6.	Typical Non-Critical Response	12
7.	Typical Critical Response	12

BASE- HEATING RESEARCH REVIEW

by Homer Wilson

		Page
	SUMMARY	14
I.	INTRODUCTION	14
II.	SHORT-DURATION TECHNIQUE	15
III.	EXTERNAL-FLOW REYNOLDS NUMBER PROGRAM	16
IV.	FLOW-FIELD VISUALIZATION	17
V.	RADIATION	18
VI.	INVESTIGATION OF COMBUSTION OF HYDROGEN IN A HYPERSONIC AIRSTREAM	19

LIST OF ILLUSTRATIONS

Figure	Title	Page
1.	Variation of Radiative and Convective Base Heating with Altitude for Various Configurations	14
2.	Combustor Schematic, Supply Tube-Tank Wave Diagram and Installation	15
3.	Data Obtained Using Short Duration Techniques of Various Engine Configurations	16
4.	Data Obtained with Short-Duration Techniques	16
5.	Schematic of External Flow Facility with some Typical Pressure Traces	17
6.	Results from Flow-Field, Visualization Study	18
7.	Comparison of Experimental Data with "Band Model" Results for Water Vapor	19
8.	Mixing of Hydrogen Jet with Vehicle Boundary Layer	19

RAREFIED-GAS DYNAMICS

by James O. Ballance

		Page
	SUMMARY	21
I.	INTRODUCTION	21
II.	PRESSURE PROBE CHARACTERISTICS	22

		Page
III.	AERODYNAMIC COEFFICIENTS	23
IV.	JET-SPREADING CHARACTERISTICS	23
V.	SURFACE-PHYSICS STUDIES	24
VI.	EXPERIMENTAL FACILITIES	25
	REFERENCES	25

LIST OF ILLUSTRATIONS

Figure	Title	Page
1.	Mean-Free Path of Air at Various Altitudes	21
2.	Flow Regimes for Rarefied-Gas-Flow	22
3.	Molecular-Flow Rate through Duct as a Function of Duct Length to Radius Ratio, L/R	22
4.	Transmission Probability for Tubes at Zero Angle of Attack for Various Speed Ratios	23
5.	Transmission Probabilities for Orifice Restricted Tube at Various Angles of Attack	23
6.	Drag Coefficient, $T_w/T = 0.4$	23
7.	Normalized Transmission Probabilities as a Function of Knudsen Numbers for L/A Values of 0.2, 0.5, 1.0 and 2.0	24

TURBULENT FLUCTUATION MEASUREMENTS WITH THE CROSSED-BEAM METHOD

by F. R. Krause, M. J. Fisher, and R. E. Larson

		Page
	SUMMARY	26
I.	INTRODUCTION	26
II.	OPTICAL INTEGRATION OVER CROSS-CORRELATION AREAS	26
III.	APPROXIMATION OF POINT MEASUREMENTS	27
IV.	EXPERIMENTAL RESULTS	28
V.	FUTURE APPLICATIONS	31
VI.	CONCLUSIONS	34
	REFERENCES	34

LIST OF ILLUSTRATIONS

Figure	Title	Page
1.	Optical Integration over Wave Fronts in Turbulent Flows	27
2.	Turbulence Scales and Intensities from Crossed-Beam Covariance Measurements	28
3.	Local Power Spectra Convection Speeds and Eddy Lifetimes from Crossed-Beam Correlation Measurements	28
4.	The First Crossed-Beam Correlator	29
5.	Light Source and Detector Arrangement	29
6.	Convection Velocity from Crossed-Beam Correlation	30
7.	Convection Velocity from Crossed-Beam Correlation	30
8.	Comparison of Radial Distribution of Convection Velocity	30
9.	Measurement of Eddy Scales	30
10.	Turbulent Intensity Profiles	31
11.	Turbulent Fluctuations of Base Pressure and Heat Transfer Rates	31
12.	RMS Velocity Profiles in Two-Dimensional-Base Flow with and without Wall Effect	32
13.	Supersonic Noise Sources in a Single F-1 Engine Jet	32
14.	Recirculation Zone Flow Field	33

INTRODUCTION TO RESEARCH ACHIEVEMENTS REVIEW ON AERODYNAMICS RESEARCH

By

Dr. E. D. Geissler*

The subjects in this aerodynamics review are varied and cover such topics as prediction methods of drag and lift characteristics, jet penetration in water, base-flow phonomena, optimum nose shape design and several topics related to aerodynamic measurements. The paper by Dr. F. Krause discusses a very promising new optical cross-correlation method. If the expected results of this method materialize, the state-of-the-art of some aerodynamic measurement techniques will be advanced markedly.

Dr. Platzer's contribution concerns some major research activities in unsteady aerodynamics, a field which represents still several ticklish problems for the Saturn program (in particular, aerodynamic noise-and-ground-wind oscillation). Mr. Homer Wilson reports on aerothermodynamic research studies, primarily base heating, which is not yet in a very satisfactory shape in spite of substantial experimental efforts. This is particularly true when it is necessary to predict new configurations.

A final paper by Mr. Jim Ballance gives a short discussion of studies on rarefied-gas dynamics - a topic which, while not yet so prominent in producing engineering headaches for the designers of space vehicles, will undoubtedly be of growing concern with extended stay time in very high altitudes and which especially poses many unsolved questions concerning instrumentation.

The activities reported are all carried out with participation and supervision of personnel of the Aerodynamics Division, even though a major share is done by contractors in Government and industry. It is hoped that these presentations will succeed in impressing the reader with the scope and importance of aerodynamics research in space-vehicle design and will also illustrate the particular flavor of applied aerodynamic research which is in close connection with the development of space vehicles. Problems are stimulated by the need for practical answers and sometimes by results from flight tests rather than selected according to their academic appeal. The justification of aerodynamic research facilities at the vehicle development agency, besides the larger aerodynamic research center facilities, stems from similar reasons and appears amply demonstrated by efficiency in tackling immediate problems.

Aerodynamics of space vehicles are relatively unglamorous compared with, for example, development of power plants. With increasing size of vehicles, the immediate importance of aerodynamic forces versus inertial effects decreases. Whereas the performance of an airplane is the result of a direct balance between aerodynamic drag and lift characteristics versus available thrust, the performance for a big space vehicle is mainly defined by propulsive inertial balance. However, it must be kept in mind that the efficiency of the structural design causes increasing concern with increasing rocket size and this structural design is strongly influenced by aerodynamic loads (i.e., bending loads, necessary control forces, aerodynamic noise, base heating). The efficient design frequently favors shapes which are not conducive to undisturbed flow characteristics (protuberances and separation including geometry) and requires prediction of flow not encountered in airplane work.

* Director, Aero-Astrodynamics Laboratory.

GENERAL REVIEW OF AERODYNAMICS RESEARCH

By

Werner Dahm

I. INTRODUCTION

The scope of aerodynamics research at MSFC is determined by the fact that, in accordance with the Center's mission, it has to serve space-vehicle development, and especially launch-vehicle development. Under this guideline, this work includes: (a) development or improvement of analytical methods, and their adaptation to our needs; (b) experimental investigations; (c) development and improvement of experimental methods and facilities; (d) development of instrumentation and probing tools; and (e) general design studies.

As a further guideline, tasks which do not promise useful design applications within a period of about 5 years are considered beyond MSFC's scope. The majority of the tasks yield results which are applied within a much shorter period.

The following are some typical examples of our research work; some other areas will be covered in separate papers.

(a) Subsonic flow.

(b) Jet impact in water.

(c) Base-flow investigation.

(d) Effect of wall-to-total temperature ratio on hypersonic flow detachment.

(e) Variable porosity walls.

(f) Dynamic balance for Saturn forebody.

II. SUBSONIC FLOW

The aerodynamic characteristics of the Jupiter nose cone which are shown in Figure 1 are examples of the analytical work. This example is concerned with pressure and lift distribution on bodies of revolution in subsonic flow. The bodies which are dealt with always have a blunt base, a case which available theories could not properly handle. Therefore, a method was developed which consists of distributing singularities on the surface of the body, and using the special boundary condition that the rim-base pressure is equal to the base pressure, and that the local lift is zero. The base pressure cannot be given by inviscid theory, and must be known a priori; the zero-lift condition is an equivalent of the kutta-condition of wing theory, and reflects the fact that virtually no pressure difference can be maintained across the "dead air" of the wake.

Figure 1 compares analytical and experimental results on a blunt-nosed cone. A blunt-nosed cone was selected because a complete set of experimental data were available, and because the base-effects are fairly pronounced. The zero-lift pressure distribution in the lower left corner coincides with the experimental results of Figure 1. This is also true for the lift distribution in the upper left corner of Figure 1. At this particular Mach number, lift and pressure over the rear 20 percent of the body are noticeably influenced by the base. As the Mach number decreases, the base influence extends further forward, and lift is lost on the rear of the body. The corresponding effects on the total lift and center of pressure can be seen on the 2 graphs on the right of Figure 1. Since the method correctly describes the flow field near the base including the effects of the base pressure, the effects of the rocket jets on the vehicle stability can be estimated once the base pressure with jets on is known.

Figure 2 shows another example of the application of this method in that it depicts the drag of cones with tip half angles from 15° to 90° as function of the base pressure. The experimental points were obtained from a water tunnel, where the base pressure is fixed by the cavitation conditions; therefore, the base pressure coefficient can be varied. Agreement between analyses and experimental results is very good. Closer inspection shows that the total drag varies less than the base drag, reflecting again the forward effect of the base pressure. Incidentally, the analysis yields a correct description of the major part of the cavitation bubble. This result is of interest to submarine applications; to us, it is only an interesting by-product.

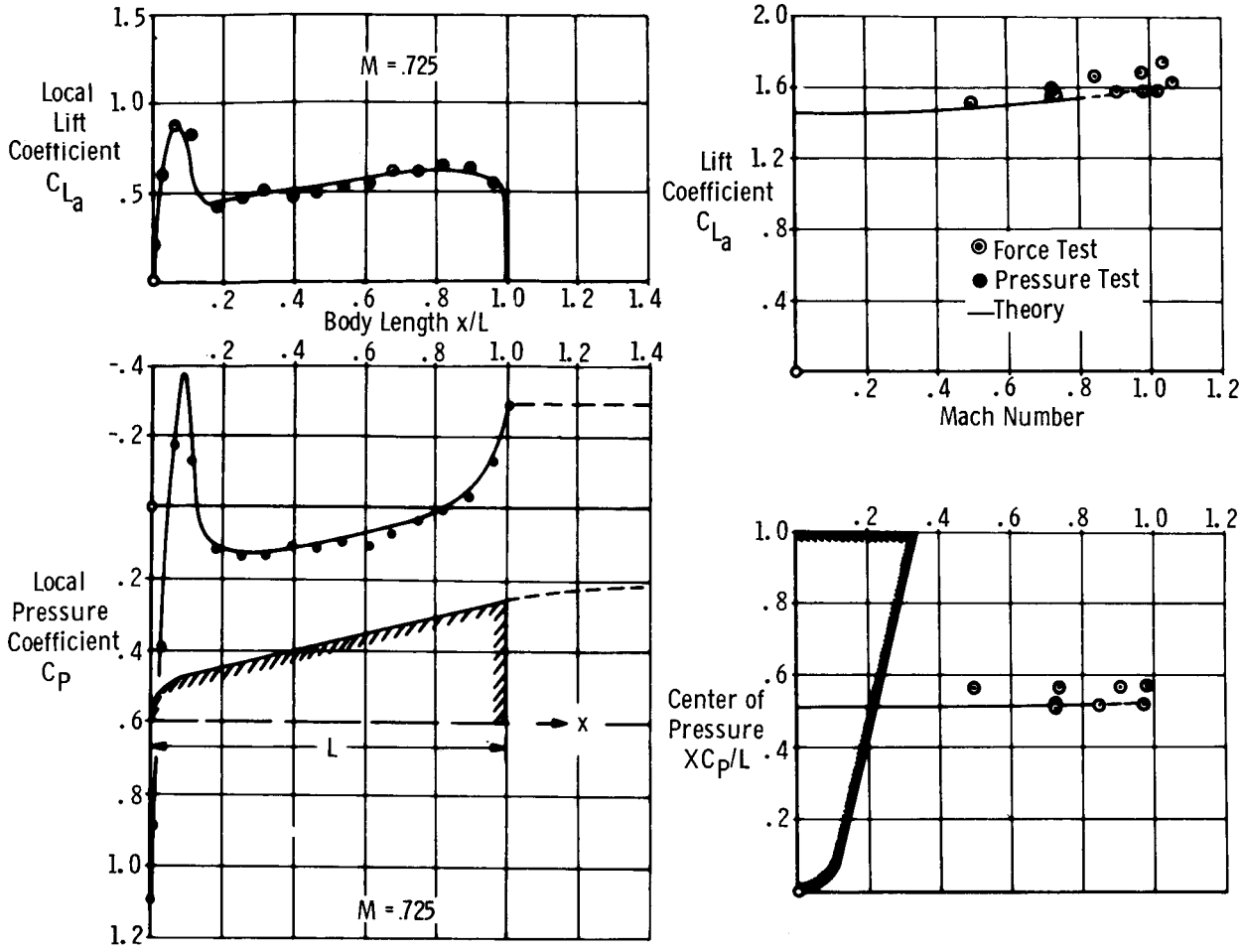

FIGURE 1. PRESSURE DISTRIBUTION ABOUT A JUPITER NOSE CONE

III. JET IMPACT IN WATER

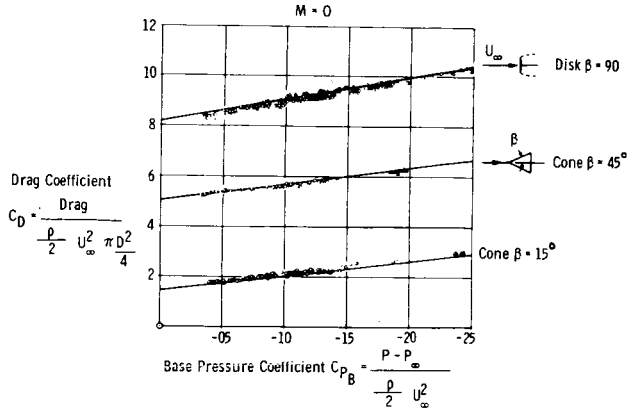

FIGURE 2. DRAG COEFFICIENT OF CONES OF DIFFERENT APEX AS A FUNCTION OF THE BASE PRESSURE COEFFICIENT

Jet penetration into water represents another example of our analytical work (Fig. 3). There are a number of reasons why launch facilities should be placed in the offshore waters such as launch-site real estate requirements. In this case the rocket jets would be discharged into the water, and it is necessary to know how deeply they penetrate. Scale-model simulation is practically impossible (it would require testing in a low-pressure chamber, or on a rocket sled under controlled, high acceleration). Therefore, the question has been attacked by composing a simple, approximate model of the process, and by checking the validity of this model with the results of small-scale jet tests. The model which was used was the well-known variation of the impact pressure of turbulent free jets with the distance downstream of the nozzle exit, and the fact that: (a) the penetration depth must correspond to the local impact

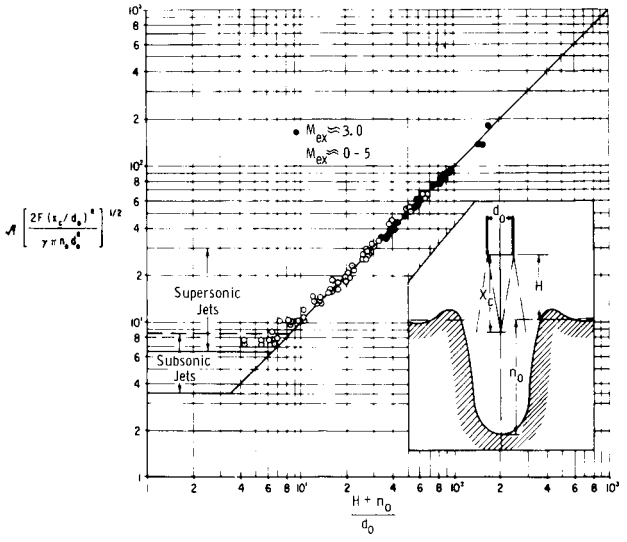

FIGURE 3. PENETRATION DEPTH OF SUB AND SUPERSONIC JETS IN WATER

pressure of the jet; and (b) the buoyancy of the cavity volume should equal the thrust of the engine. Figure 3 shows the correlation of a sizeable number of experiments with hot and cold subsonic and supersonic jets, using the resulting relations. The abscissa represents the distance of the apex of the cavity from the nozzle exit. The ordinate contains the thrust F, the specific weight of the liquid γ, the jet diameter d, the length of the inviscid jet core x_c, the penetration depth n_o, and a Mach number function. The horizontal lines correspond to cases where the inviscid core of the jet hits the bottom of the cavity. The inclined line corresponds to cases where $H + n_o > x_c$, i.e., where the "inviscid core" of the jet no longer reaches the bottom of the cavity. The correlation of the data in Figure 3 shows inherently that the presence of the water has essentially no effect on the impact pressure profile of the jet. The meaning of these data may be illustrated by an application to the F-1 engine.

	H	n_o
F-1 engine:	0	160' = 50 m
	100' = 30.4 m	93' = 28 m

For closely clustered jets, the penetration depth is somewhat larger than for single jets and can be estimated from a model test of the impact pressure profile in free air.

IV. BASE FLOW INVESTIGATION

The various base-heating problems encountered in high speed reentry as well as from our engine jets have, for a long time, aroused our curiosity about what really goes on in the so-called "dead-air zone" at the base. These processes have been studied on a two-dimensional, blunt based wing model at M = 3 with a turbulent boundary layer. Figure 4 shows a shadowgraph picture of the base area of this model. The white rectangle on the left is the rear end of the model, 15 inches (37.1 cm) high. The traces of the boundary layer, the Prandt-Meyer fan, the free shear layers, the tracking shocks, etc. can also be seen. Heat transfer and pressure distribution tests have been made on the base plate. The recirculation field, the free shear layers, and the base plate boundary layer have been probed with total pressure and temperature probes, wind vanes, an interferometer, and hot-wire anemometers. The lower part of Figure 4 shows the density and distribution at zero heat flux, taken from an interferometer test. The flow in the recirculation zone was found to be extremely turbulent, with $\sqrt{u'^2} = 0(\bar{u})$. The wind-vane tests of the mean velocity directions, shown by the arrows in the upper parts of Figure 4, deteriorated near the model centerline, indicating large outward flow angles rather than the required direction parallel to the centerline. The presumed cause is the high level of turbulence combined with strong shear flow effects. The main resistance to the heat transfer was found vested in a very thin base plate boundary layer, about 0.06 inches (0.152 cm) thick; the free shear layers played only a minor role. Outside of this base boundary layer, the total temperature is constant throughout the recirculation zone and the inner part of the shear layers. The base boundary layer is unlike any ordinary boundary layer. Its temperature profile seems to consist essentially of two straight lines, an outer one of small gradient dt/dx, and an inner one with steep gradient, which corresponds to the molecular heat transfer and reflects the existence of a laminar sublayer whose thickness is 0.005 inch (0.0127 cm). The cause of this peculiar profile is believed to be the extreme turbulence level of the recirculation zone. Figure 5 shows the effect of the base plate temperature on T_b, the total temperature in the recirculation zone. T_b is seen to be very little affected by the base plate temperature T_w. dT_b/dT_w indicates the distribution of the resistance to the heat flux between the free shear layers and the base boundary layer.

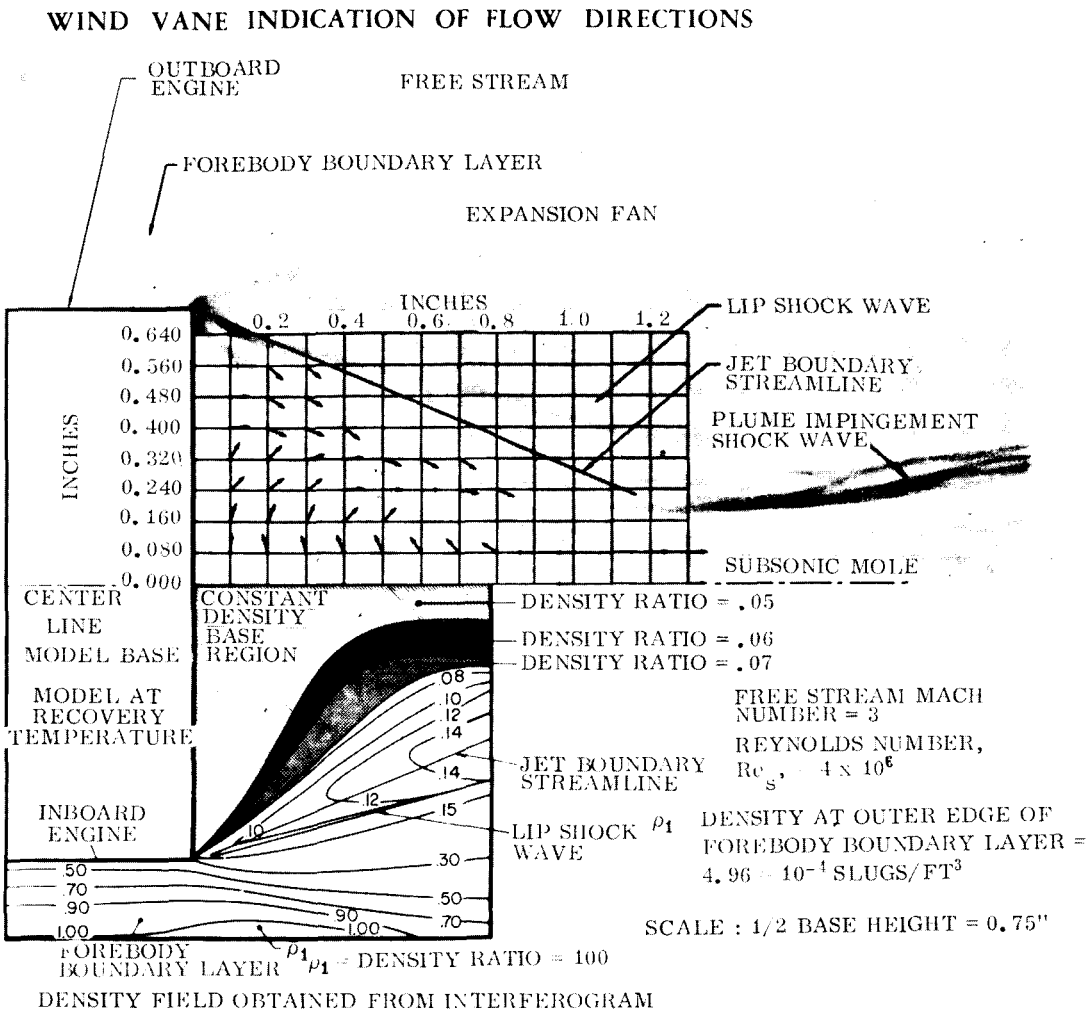

FIGURE 4. RECIRCULATION ZONE FLOW FIELD

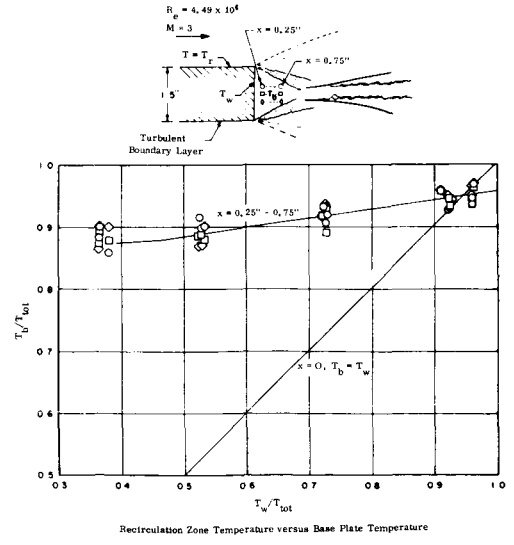

FIGURE 5. TWO-DIMENSIONAL BASE FLOW

V. EFFECT OF WALL-TO-TOTAL TEMPERATURE RATIO ON HYPERSONIC FLOW DETACHMENT

To assess factors that have to be observed for proper wind-tunnel simulation, the wall-to-total temperature ratio was varied in a wind-tunnel test of a Saturn forebody model at a Mach number of 6. Figure 6 shows schlieren pictures of the model at T_w/T_o = 0.88 and 0.22, demonstrating differences of flow detachment on the escape rocket-vehicle nose combination. Figure 7 shows the effect of T_w/T_o on the drag coefficient. At T_w/T_o near 1, the flow is fully detached and the drag is low. As the wall temperature decreases, the flow detachment recedes, increasing C_D, until the flow is fully attached and C_D has reached

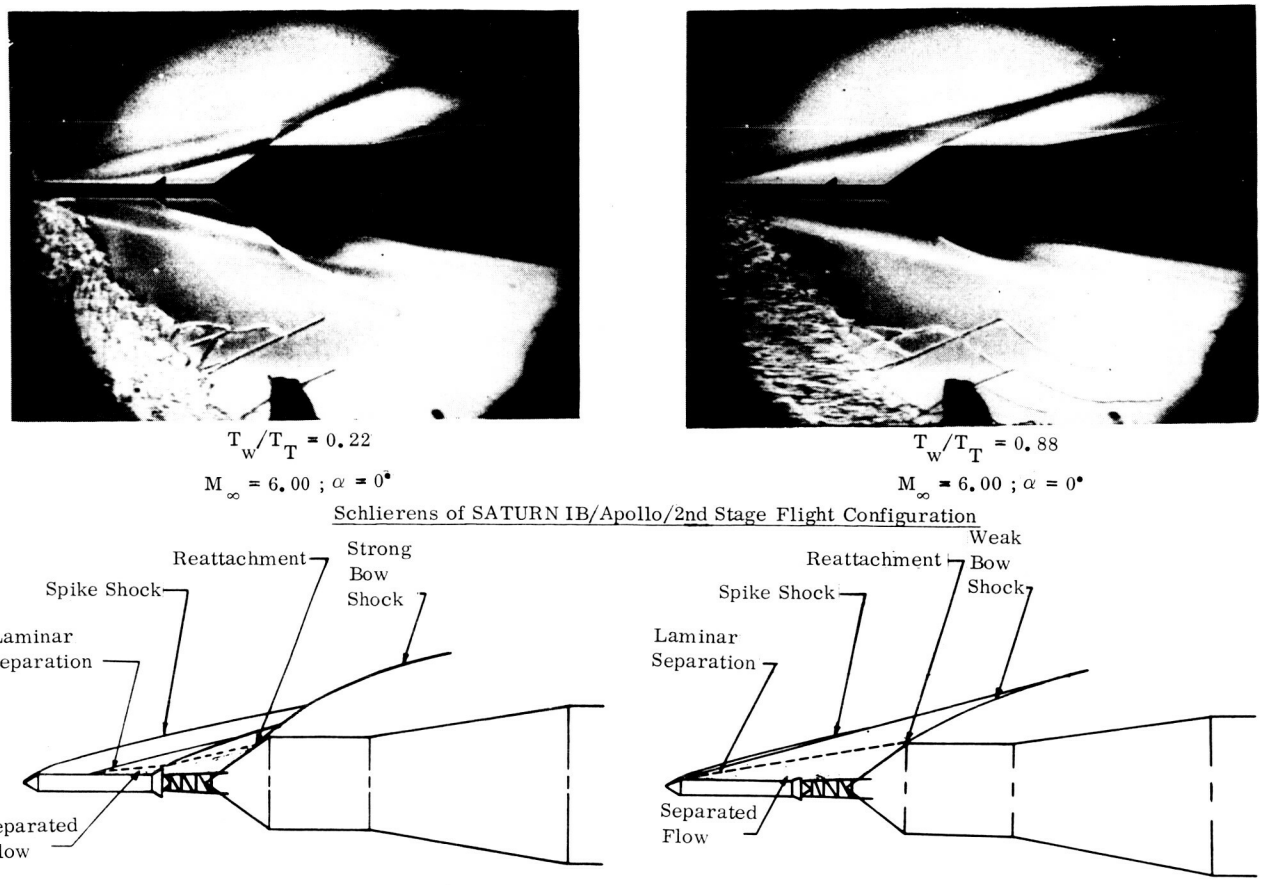

Effect of Temperature Ratio (Tw/T_T) on the Aerodynamic Flow Fields for Trajectory Reynolds Number Conditions

$Re_{Dia} = 0.22 \times 10^6$ (Trajectory) ~ D_{Ref} = 257"

FIGURE 6. SCHLIEREN PICTURES OF THE MODEL AT T_w/T_o = 0.88 AND 0.22

its maximum. A similar increase of C_D is obtained by a moderate increase of the Reynolds number. Therefore, it is believed that the observed reaction of the flow to T_w/T_o is caused by effects of the temperature ratio on boundary layer transition. The results indicate that under proper circumstances T_w/T_o must be observed as a similarity parameter.

VI. VARIABLE POROSITY WALLS

The MSFC 14 × 14-inch (35.56 × 35.56-cm) Trisonic Wind Tunnel uses a transonic test section with perforated walls. Use of perforated walls to reduce the wall interference is an accepted practice. Figure 8 shows a typical test section of this type. Normally, one fixed type of wall perforation is used throughout the transonic range, rather than perforations adapted individually to each Mach number. The price for this simplification is a reduced data accuracy. Our Facilities Branch has, therefore, developed walls of variable porosity (Fig. 9). They permit a change of the porosity by simply moving one of the two wall plates. The result is illustrated by the next two graphs. Figure 10 shows a cone-cylinder pressure distribution with fixed-porosity walls set for good average cancellation at $1.0 \leq M \leq 1.3$; Figure 11 shows the measured pressure distribution on the same body with our variable porosity walls set for optimum cancellation at this Mach number.

Outside agencies are becoming interested, i.e., LeRC, AEDC.

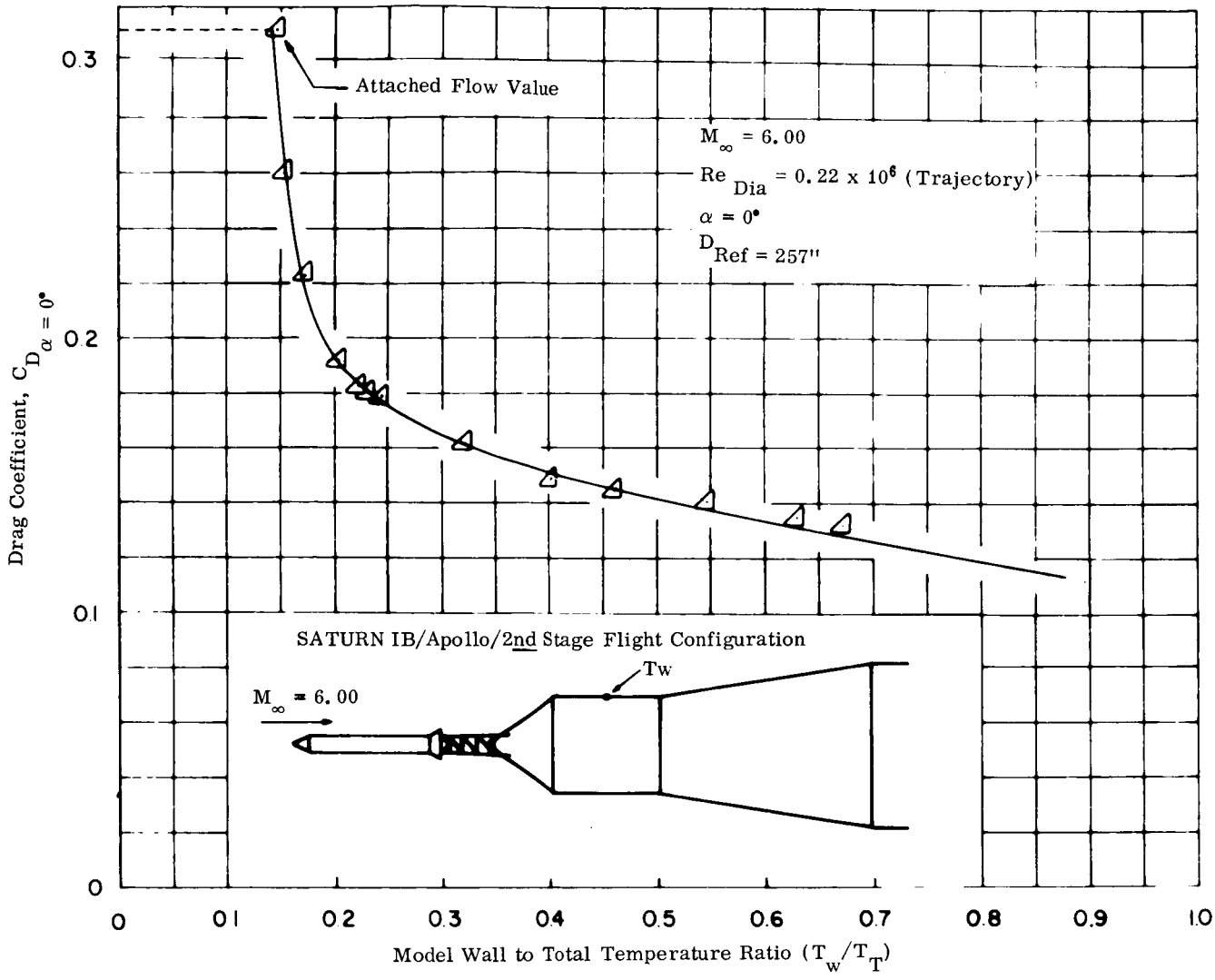

Variation of Drag Coefficient with Temperature Ratio (T_w/T_T) for Trajectory Reynolds Number Conditions

FIGURE 7. THE EFFECT OF T_w/T_o ON THE DRAG COEFFICIENT

VII. DYNAMIC BALANCE FOR SATURN FOREBODY

The aerodynamically unfavorable nose shape of the Saturn vehicles may give rise to dynamic bending instabilities. To perform wind-tunnel tests on these effects, a sting-mounted dynamic balance (Fig. 12) was designed. The balance forms an integral part of the model since its frame supports and stiffens the light external shell. This balance permits measurements at preselected frequencies ≤ 100 Hz, angles of attack, and amplitudes of ± 2½ degrees about the center of rotation. The frequencies are limited by stresses in the escape tower of the model. Preliminary tests in the transonic range proved that low internal damping was achieved. The aerodynamic damping is 70 to 85 percent of the total damping measured. The balance requires only simple electronic equipment, and permits high acceleration due to its ample torque and power.

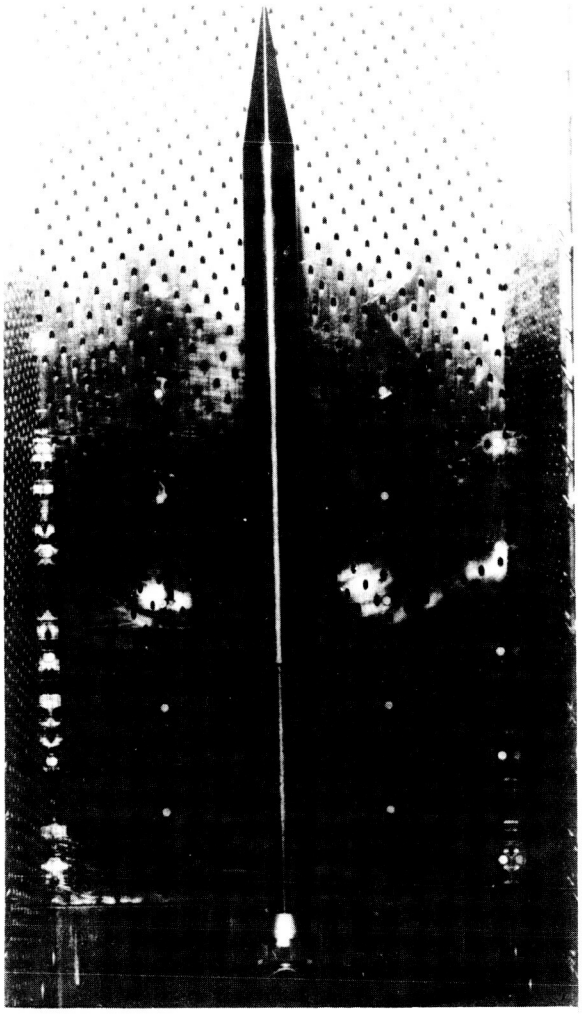

FIGURE 8. PHOTOGRAPH OF 20° CONE-CYLINDER IN TUNNEL

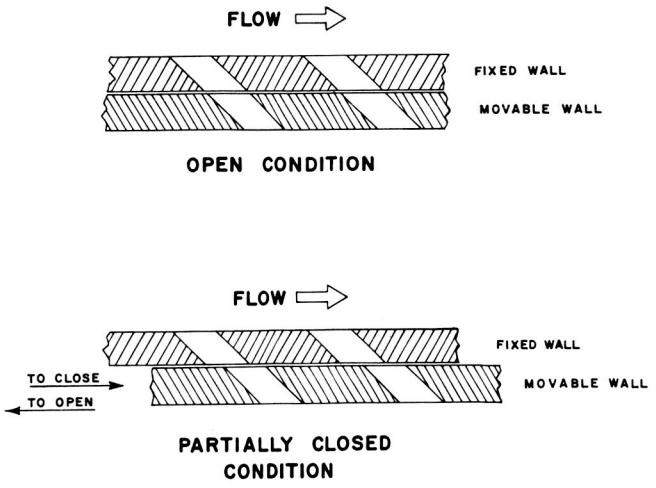

FIGURE 9. SKETCH OF VARIABLE POROSITY CONCEPT

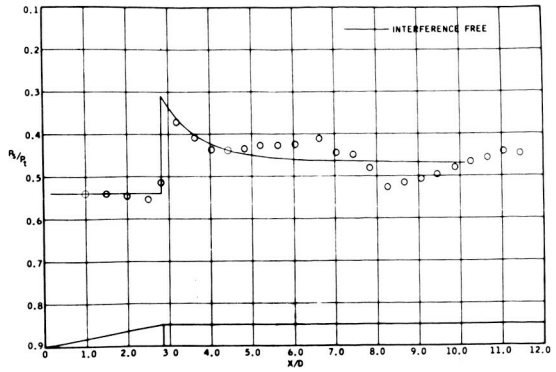

FIGURE 10. CONE-CYLINDER PRESSURE DISTRIBUTION AT M = 1.10 WITH A FIXED TUNNEL WALL POROSITY OF 7.5 PERCENT WITH 60° SLANTED HOLES

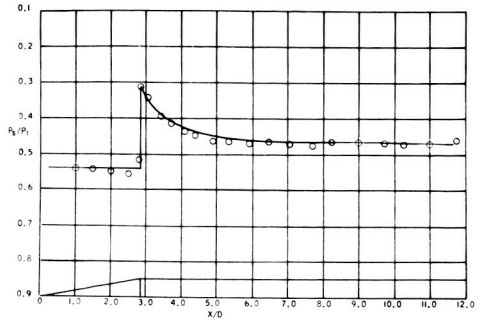

FIGURE 11. CONE-CYLINDER PRESSURE DISTRIBUTION AT M = 1.10 WITH VARIABLE POROSITY WALLS SET AT 1.6 PERCENT WITH 60° SLANTED HOLES

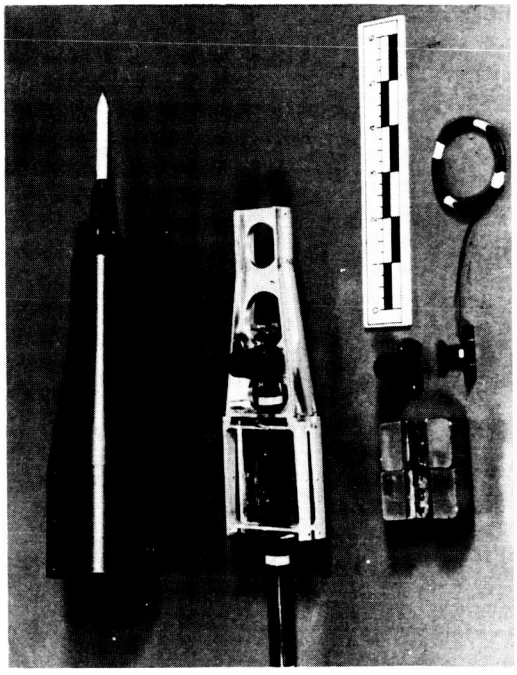

FIGURE 12. STING, MOUNTED DYNAMIC BALANCE

UNSTEADY AERODYNAMICS

By

M. F. Platzer

SUMMARY

This study briefly describes some of the problem areas in the Saturn-launch-vehicle-development program that are related to unsteady phenomena. The two principal types of unsteady phenomena are self-excited phenomena and externally-excited phenomena. Self-excited phenomena consist of panel flutter, body flutter, and fin flutter. Studies conducted in this area show that strong influences are exerted by the boundary layer. Concurrently, studies are being made to calculate the nonlinear and the linearized-inviscid-flow over pulsating and stationary wavy-walled surfaces.

The following three methods have been initiated for predicting aerodynamic damping: a linearized-unsteady-potential equation based upon a generalized Adams-Sears iteration process; a linearized method of characteristics solution for slowly oscillating pointed-bodies of revolution that are of arbitrary profile and that are in supersonic flow; and a nonlinear method of characteristics solution.

Externally-excited phenomena consist of buffeting loads, noise problems, and meteorological environment, such as wind gusts and atmospheric turbulence. Research to determine the power-spectral characteristics of various buffeting regions is in process. Theoretical studies are also being made on the relative contribution of regions of high-entropy production in the exhaust stream to the overall intensity, propagation, and directivity characteristics of the radiated acoustic energy.

I. INTRODUCTION

Unsteady aerodynamics are airflows that are time dependent and that may produce a dynamic response of the vehicle structure or control system. A characteristic feature of these response problems is that comparatively small aerodynamic forces may produce a very large or even catastrophic dynamic response. Aircraft wing flutter and the Tacoma Narrows Bridge failure are typical examples.

Unsteady phenomena can be divided into the general classes of self-excited and externally-excited phenomena. Self-excited phenomena shall consist of:

(a) Panel flutter.

(b) Body flutter.

(c) Fin flutter.

Externally-excited phenomena shall consist of:

(a) Buffeting loads.

(b) Noise problems.

(c) Meteorological environment, such as wind gusts and atmospheric turbulence.

The primary objective of this study is to describe the efforts to provide an accurate description of unsteady aerodyanmic forces to be used to furnish input information to the structures' and control systems' designer. No established procedures exist for determining an unsteady aerodynamic environment in connection with space vehicles or missiles. Therefore, this study is primarily of a research nature. However, these research results should be converted into useful design information as soon as possible.

II. PANEL FLUTTER

Panel flutter is the self-excited oscillation of a panel in a flow under the action of aerodynamic forces generated by the panel motion. The possibility of panel flutter was suspected in the early phases of the V-2 development. Since then, experiments have shown conclusively that flutter of surface skin panels can exist. Wind-tunnel tests showed that a traveling, wave-type, flutter condition caused panel failure within a period of a few seconds [1]. Recently, panel flutter occurred on the X-15 airplane as shown in Figures 1 and 2. In general, structural nonlinearities tend to limit the flutter amplitudes and, therefore, cause the modes of structural failure to be related to

fatigue rather than to the explosive fracture of the skin surface. However, it is quite dangerous to regard panel flutter only as a fatigue problem. Tests of the corrugation stiffened X-15 panels, e.g., revealed that flutter was very sudden and very severe. The panels failed unless flutter was stopped within a period of a few seconds.

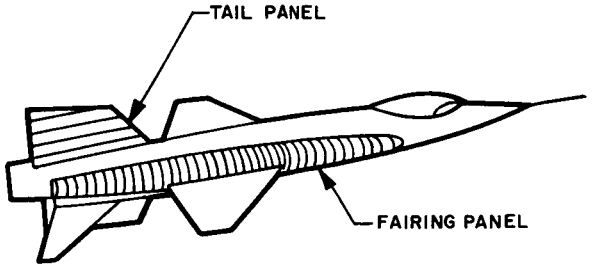

FIGURE 1. REGIONS OF X-15 RESEARCH AIRCRAFT AFFECTED BY PANEL FLUTTER

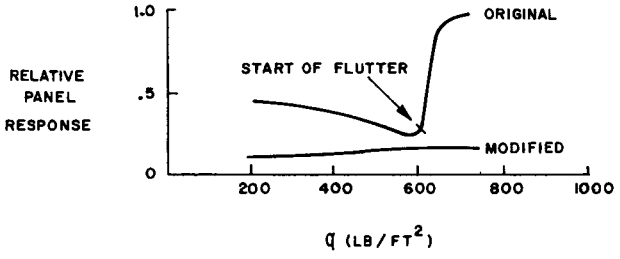

FIGURE 2. VARIATION OF PANEL-RESPONSE ENVELOPE WITH DYNAMIC PRESSURE OBTAINED FROM FLIGHT MEASUREMENTS ON AN X-15 SIDE-FAIRING PANEL

For this reason, it was considered necessary by the Aero-Astrodynamics and the Propulsion and Vehicle Engineering Laboratories to test the hat sections of the Saturn-IC stage. These tests, which were carried out by Boeing personnel in the Ames Research Center (ARC) 2- and 11-foot (0.61- and 3.35-m) tunnels, demonstrated the strong influence exerted by the boundary layer.

Theoretical-flutter calculations are based upon inviscid-linearized-flow theory. Only recently has the need for taking into account the effect of the viscous boundary layer been recognized. For this reason, the Unsteady Aerodynamics Branch has initiated a cooperative research program with ARC and Georgia Institute of Technology to study the influence of the boundary layer on panel flutter. A decision was made to first explore the stationary flow over wavy-walled surfaces for varying boundary layer thicknesses. The first test in this program was scheduled for January 1966 at the ARC 2-foot (0.61-m) tunnel. The Mach number range to have been explored was $0.8 < M < 1.6$. Concurrently, theoretical-inhouse studies are being carried out to calculate nonlinear- and linearized-inviscid flow over pulsating and stationary wavy-walled surfaces [2].

III. AERODYNAMIC-DAMPING STUDIES

As a result of the increased flexibility of the launch vehicles in the Saturn class, it has become necessary to investigate the aerodynamic damping characteristics of these vehicles during flight in the first three bending modes. Theoretical approaches to predict the aerodynamic damping are especially important because the simulation of elastic vehicle response in a wind-tunnel test is very complicated, and the results of this expensive test may be of limited value due to the wind-tunnel noise and the model-mount interference. Another factor in favor of the theoretical approach is that the elastic model usually necessitates a lead time of 1 year. Consequently, the test results become available when the vehicle design has been frozen.

For these reasons, the Unsteady Aerodynamics Branch tried to formulate theoretical approaches to predict the aerodynamic damping. These theoretical approaches had to be based upon inviscid-attached-flow concepts in order to make the problem mathematically tractable. So far, the following results have been obtained:

(a) A solution of the linearized unsteady potential equation has been worked out based upon a generalized Adams-Sears iteration process. This work is now complete [3] and Figure 3 shows one result that demonstrates the influence of body shape and Mach number upon the pitch damping coefficient.

(b) A linearized method of characteristics solution is presently being investigated for slowly oscillating pointed bodies of revolution that are of arbitrary meridian profile and are in supersonic flow. This method is an extension of the Oswatitsch-Erdmann characteristics method. Preliminary results for the steady case show a wide applicability [4].

(c) A nonlinear method of characteristics solution is being investigated by the Massachusetts Institute of Technology (MIT). This approach is based upon the superposition of small time-dependent angle of attack perturbations on a nonlinear-axisymmetric-flow field that is determined by the method of characteristics. Good results have been obtained for the oscillating cone [5].

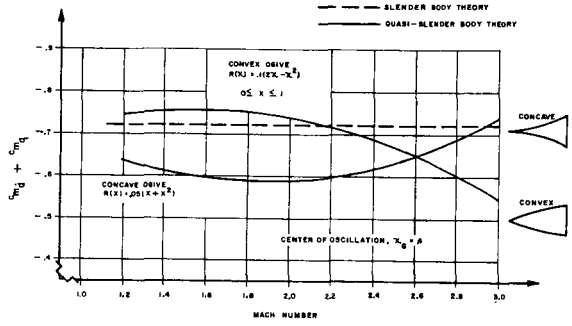

FIGURE 3. EFFECT OF MACH NUMBER ON FIXED AXIS DAMPING IN PITCH MOMENT COEFFICIENT FOR CONVEX AND CONCAVE PARABOLIC OGIVE OF THICKNESS RATIO 0.1

Calculation of damping characteristics, which are based upon attached flow concepts, are not sufficient for most of the current, launch-vehicle configurations. Blunt nose cones and steep interstage flares, which have become characteristic of space boosters, produce large regions of flow separation that dominate the aerodynamic loading over the vehicle in the transonic and the supersonic speed range, as shown in Figure 4. As a result, it has become necessary to take into account separated flow effects upon aerodynamic damping. The success of an analytical and experimental method of dynamic analysis of the Atlas-Able launch vehicles [6] suggested a possible adaptation to the Saturn-launch-vehicle configuration. This method is based upon the assumption that the total lift force on any part of the vehicle consists of the following components:

(a) Local lift, which is lift due to local motion at time t.

(b) Induced lift, which is lift induced by the wake created at the nose at time t-Δt.

This suggests that local lift is always in phase with the lateral vehicle motion and that induced lift is out of phase by the time lag Δt. These two assumptions make it possible to determine aerodynamic damping from static-wind-tunnel tests thus eliminating expensive elastic model tests. This procedure is being applied to the various Saturn-launch-vehicle configurations.

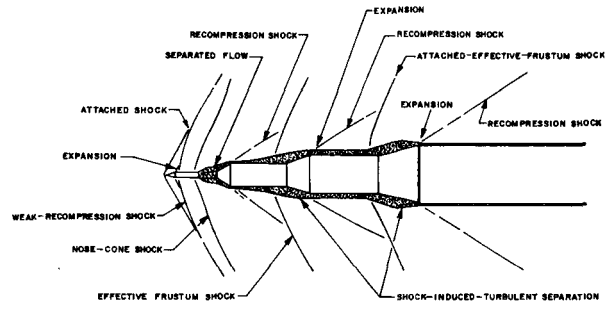

FIGURE 4. FLOW FIELD ABOUT TYPICAL SATURN SERIES VEHICLE

IV. BUFFETING

Buffeting is the pressure oscillation caused by separated flow. The launch-vehicle-interstage areas may cause intensive fluctuating pressures, and, consequently, severe structural loads as shown in Figure 5. In the separated flow region shown in Figure 5, a slowly circulating-reverse flow exists, overlain by a free-shear flow. The highest fluctuating pressure levels are found to occur at the point of flow separation and reattachment. Current research is devoted to the determination of the power-spectral characteristics of these buffeting regions. The Unsteady Aerodynamics Branch has several research programs to analyze this problem. Perhaps the most significant program in this field is the protuberance-wind-tunnel test which is being carried out in cooperation with ARC. This program is currently in the data reduction process and the results should be available in the near future.

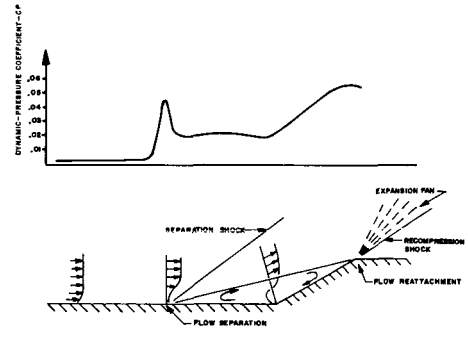

FIGURE 5. TYPICAL FLUCTUATING PRESSURE ENVIRONMENT FOR VEHICLE INTERSTAGE TYPE GEOMETRIES

V. ENGINE-GENERATED NOISE

Research in the field of engine-generated acoustics has been directed towards the determination of the predominant noise generation mechanisms in high-temperature, rocket-exhaust flows. Present investigations include theoretical studies of the relative contribution of regions of high entropy production in the exhaust stream to the overall intensity, propagation, and directivity characteristics of the radiated energy. This work is being supplemented by experimental rocket exhaust studies using a substitute gas to simulate the predominant flow characteristics of the H-1 engine at a considerably lower temperature, thus allowing measurements to be made in the flow.

VI. GROUND-WINDS PROBLEM

A launch vehicle erected on the launch pad before lift-off is exposed to surface winds that may generate large dynamic loads under certain circumstances. Downstream from the body, a wake flow is created that is Reynolds number dependent and has characteristics which are difficult to describe mathematically. In certain cases, the well known Karman vortex street is obtained. At the higher Reynolds numbers, the vortex shedding is very dependent upon the type of flow in the vicinity of the body (laminar- or turbulent-boundary layer). Therefore, a distinction must be made between subcritical and supercritical flow regimes. Insufficient understanding of the mechanisms involved and lack of reliable calculation methods force most investigators to extract the aerodynamic forcing function from an analysis of the aeroelastic response of various launch-vehicle configurations. The Unsteady Aerodynamics Branch has initiated an extensive wind-tunnel program on the different Saturn I, IB, and V configurations. Most of these tests are conducted at the Langley Research Center (LRC) and require aeroelastic models of about 5-percent scale. Unfortunately, for the Saturn V configuration, a full-scale Reynolds number cannot be simulated, thus introducing a further degree of uncertainty. Typical vehicle responses are shown in Figures 6 and 7. In both figures the vehicle base bending moment, due to steady drag, dynamic drag, and dynamic lift, is plotted versus the wind velocity. A typical noncritical response is shown in Figure 6, while a typical critical response due to dynamic lift at a specific wind velocity is shown in Figure 7.

The critical response is of primary concern to the vehicle designer since it may impose exceedingly high loads upon the vehicle. Unfortunately, the reason for the occurrence of such a critical response is little understood. The possibility for self-excited vibrations cannot be excluded at this time. Therefore, a cooperative research program between LRC, MSFC, and the Martin Company was formulated to investigate the aerodynamic forces on oscillating two-dimensional cylinders. These tests were conducted recently at LRC and the data are in the process

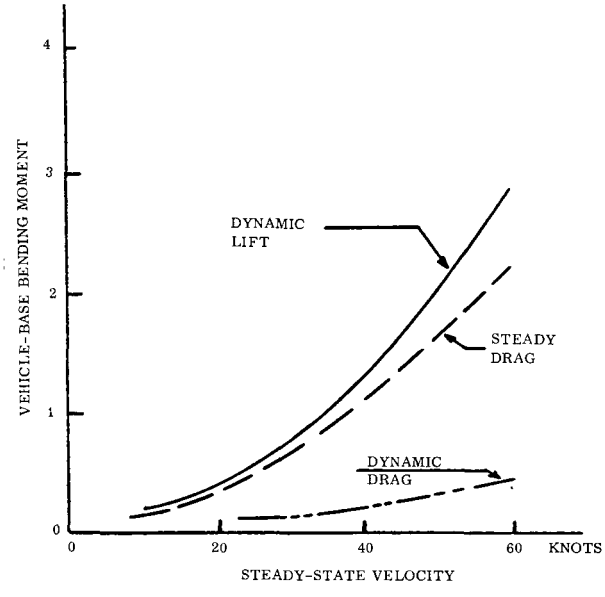

FIGURE 6. TYPICAL NON-CRITICAL RESPONSE

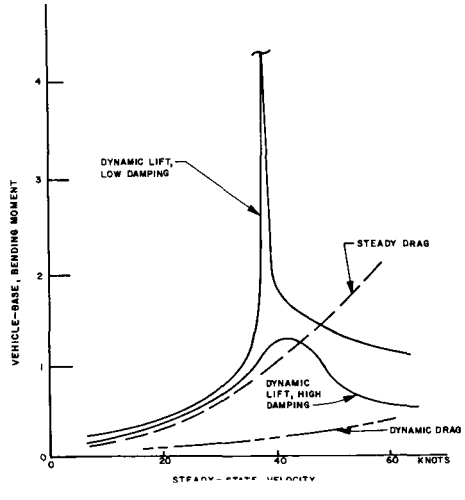

FIGURE 7. TYPICAL CRITICAL RESPONSE

of evaluation. This experimental program is being supplemented by an analytical studies program that should provide a better understanding of the basic flow-field characteristics.

Unsteady aerodynamic effects present the launch-vehicle designer with a series of important and challenging problems. Since these phenomena are little understood, a continuous and vigorous research effort is required.

VII. CONCLUSIONS

REFERENCES

1. Hermann, R.: Private Communication. University of Alabama Research Institute, Nov. 1965.

2. Platzer, M.; Beranek, R.; and Saunders, L.: On Some Aerodynamic Aspects of the Panel Flutter Problem. 3rd Aero-Astrodynamics Research Review.

3. Platzer, M.; and Hoffman, G.: Quasi-Slender Body Theory for Slowly Oscillating Bodies of Revolution in Supersonic Flow. Proposed NASA TN (MSFC, Aero-Astrodynamics).

4. Sherer, A.: Analysis of the Linearized Supersonic Flow about Pointed Bodies of Revolution by the Method of Characteristics. LMSC/HREC TM 54/20-29, TM 54/20-46, TM 54/20-63.

5. Hsu, P. T.: Solution of the Supersonic Flow Field around an Oscillating Circular Cone. MIT Fluid Dynamics Research Lab. Report No. 64-5, Dec. 1964.

6. Woods, P.; and Ericsson, L.: Aeroelastic Considerations in a Slender, Blunt-Nose, Multi-stage Rocket. Aerospace Engineering, May 1962, pp. 42-51.

BASE-HEATING RESEARCH REVIEW

By

Homer Wilson

SUMMARY

The purpose of the studies described in this report is to gain more information related to the causes and control of heating problems. To help gain this information, an external-flow facility was built to enable the Reynolds number to be varied by almost an order of magnitude; and at the same time, to provide a facility that would eliminate costly large-scale, wind-tunnel tests. Data obtained from the external-flow facility compared reasonably well with large-scale, wind-tunnel tests. By using this facility, some limited Reynolds numbers on base heating were determined. A similar, but larger and more versatile, facility has been proposed by MSFC.

This study also indicated that a flow field prevented the radiation of vehicles with clustered engine configurations from decreasing to near zero radiation as in single engine vehicles. The flow field results from an increasing altitude and decreasing ambient pressure causing the exhaust jets from the engines in a cluster configuration to expand and to impinge with the other jets in the cluster forming a shock wave. The shock waves force the exhaust gases back toward the base plate of the engine. The reverse exhaust gases will then flow radially outward between the nozzles into the atmosphere and may choke the engine at sufficiently high altitudes. This condition has caused severe heating on the Polaris and the center star areas of the Saturn vehicles.

For clustered LOX-H_2 upper-stage configurations, radiation may not be the predominant cause of heating; but it should be accurately computed since the stages fly a long period of time. In order to compute the radiation, the "band model" concept was used. To use this concept, it is necessary to know parameters such as spectral-line strength, spectral-line spacing and line half-width. Within the next year, all needed parameters are expected to be available.

Another problem studied was the dumping of combustibles along the vehicle or near the base area. If fuel-rich combustibles are entrained in the base region, large heating rates may occur. The results from the study show that upstream ejection of hydrogen can be accomplished without hazard of ignition or combustion by venting parallel to the surface through a perfectly expanded nozzle if it is displaced far enough from the vehicle to reduce hydrogen levels below flammability limits.

I. INTRODUCTION

The purpose of a research program in heating is to gain information which will improve the design of future space vehicles. The base heating problem on rocket vehicles is a combination of heating by convection and by radiation. For LOX-RP powered launch vehicles, radiation is high at sea level and decreases at higher altitudes (Fig. 1). The radiation at higher altitudes for single-engine vehicles like Jupiter decreases to near zero. Although the radiation

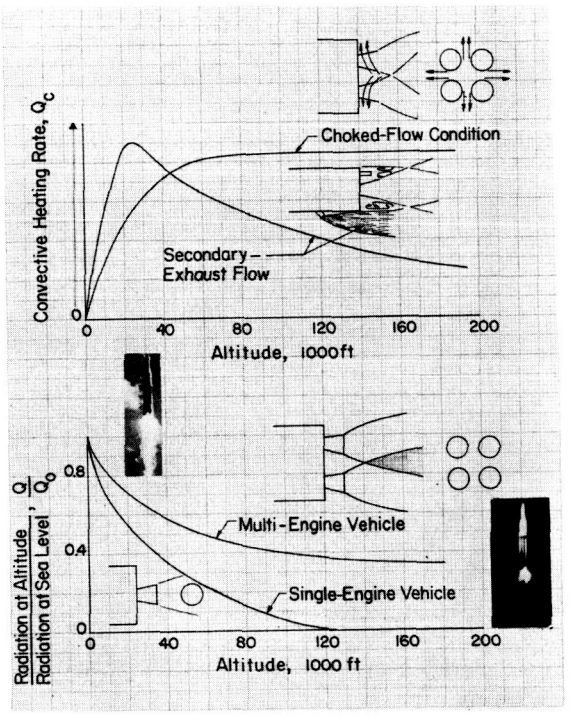

FIGURE 1. VARIATION OF RADIATIVE AND CONVECTIVE BASE HEATING WITH ALTITUDE FOR VARIOUS CONFIGURATIONS

of vehicles with clustered engine configurations is less at higher altitudes than at sea level, the impinging regions at higher altitudes apparently bring about a significant increase in the radioactive flux keeping the radiation of the vehicle from nearing zero. Upper stages powered by LOX-H_2 engines have little radiation, but the radiation should be accurately computed since the vehicles fly over a long period of time.

Convective heating for single-engine vehicles generally is small at all altitudes. For vehicles with clustered engine configurations, the impinging of the jets at high altitude sets up a recirculating flow field which causes large heating within the enclosed area.

Another problem to be reckoned with is the dumping of combustibles along the vehicle or near the base area. If fuel-rich combustibles are entrained in the base region, large heating rates may occur. These are usually a maximum in the transonic region and disappear above Mach 3 due to the absence of oxygen to support combustion.

II. SHORT-DURATION TECHNIQUE

Over the years, a wealth of flight and model data has been accumulated which was used as estimates of the thermal criteria for design purposes. Because these estimates have not been satisfactorily substantial, time has been spent on programs aimed at improving methods of generating design data and getting a better understanding of the problems. During early Saturn days, model data were obtained from scaled, long-duration, model tests. This type of testing proved costly, complex, and generally provided data over a limited range of variables. About 4 years ago, the possibility of using other techniques for obtaining model data was explored and the short-duration technique was developed. This technique is illustrated in Figure 2.

Using this technique, the propellants are stored in a pair of charge tubes and are contained by a pair of diaphragms or quick-acting valves at the end of each tube. When the diaphragms are ruptured, the gases flow into an injector, then into the combustion chamber where burning takes place. Ignition is usually by a spark plug. For high-altitude testing, the model is mounted in a vacuum tank. Testing time is determined by the time required for an expansion wave to traverse the charge tube (charge-tube length), the time required for the blast wave to travel to the tank walls and return, or the heating limitations of the model. Early results on a base plate indicate that thermal and pressure fields were established in $\frac{1}{4}$ to 1 millisecond and that several milliseconds of steady flow are available which is ample time to obtain the data.

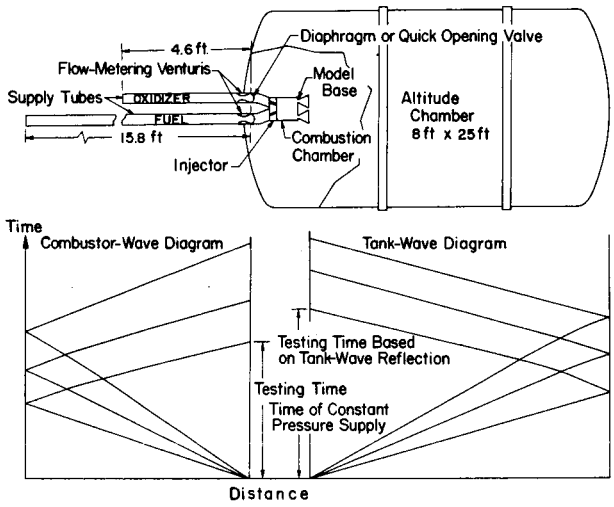

FIGURE 2. COMBUSTOR SCHEMATIC, SUPPLY TUBE-TANK WAVE DIAGRAM AND INSTALLATION

The short-duration technique has been used to obtain design data for S-IV, S-II, S-V, S-I, and Centaur stages. On a firing-to-firing basis, the short-duration technique is cheaper by an order of magnitude than the long-duration technique and provides data that compare reasonably well with long-duration model and high-altitude, flight data. The big advantage of the short-duration technique is that many variables can be easily studied. The effects of engine deflection on base heating is shown in Figure 3a for a typical, five-engine configuration. The results show that on deflecting two outboard engines toward each other by 4 degrees the maximum heating rate increases by a factor of two. This is particularly important for design of the upper stages such as S-II.

Some effects of nozzle-wall temperature on base-heating rate is shown in Figure 3b. Increasing the nozzle-wall temperature from 80 to 1000° F (26.67 to 537.78° C) results in a significant increase in base-heating rate. This results from the fact that the low-energy, exhaust gases that are reversed into the base have passed along the cooled nozzle-wall temperature.

The effect of a temperature step or discontinuity in the measurement of the film coefficient is shown in Figure 4a. Cooling the gage results in a large

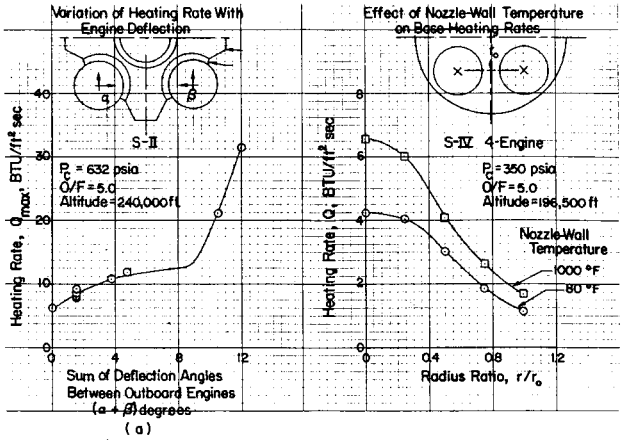

FIGURE 3. DATA OBTAINED USING SHORT DURATION TECHNIQUES OF VARIOUS ENGINE CONFIGURATIONS

increase in the film coefficient (almost a factor of two) as compared to a case where the gage temperature is equal to the plate temperature. This indicates that large errors may be present in our flight measurements where the copper-slug calorimeter temperature may be significantly different from that of the heat shield.

The effect of pressure of Reynolds number on base-film coefficient and recovery temperature is shown in Figure 4b. The initial portion of the curve shows that the film coefficient varies proportionally to the $\frac{1}{2}$ power of the pressure as would be expected for laminar flow, and the latter part of the curve shows that the film coefficient varies proportionally to the 4/5 power of the pressure as would be expected for turbulent flow. The base-recovery temperature varies proportionally to the 1/5 power of the pressure. The dependency of the recovery temperature on pressure or Reynolds number is brought about by the fact that the gases that get reversed into the base area are contained within the boundary layer of the nozzle, the state or energy level of which is primarily determined by the Reynolds number.

III. EXTERNAL-FLOW REYNOLDS NUMBER PROGRAM

In comparing model to flight data, where ambient flow effects are important, several discrepancies have occurred which seem to indicate that Reynolds number effects are present. Approximately 2 years ago, a program was initiated to build an external-flow facility which would enable the Reynolds number to be varied by almost an order of magnitude and at

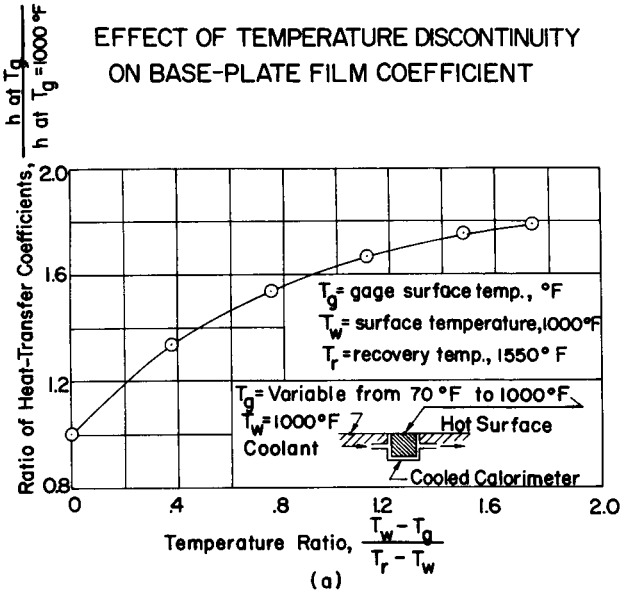

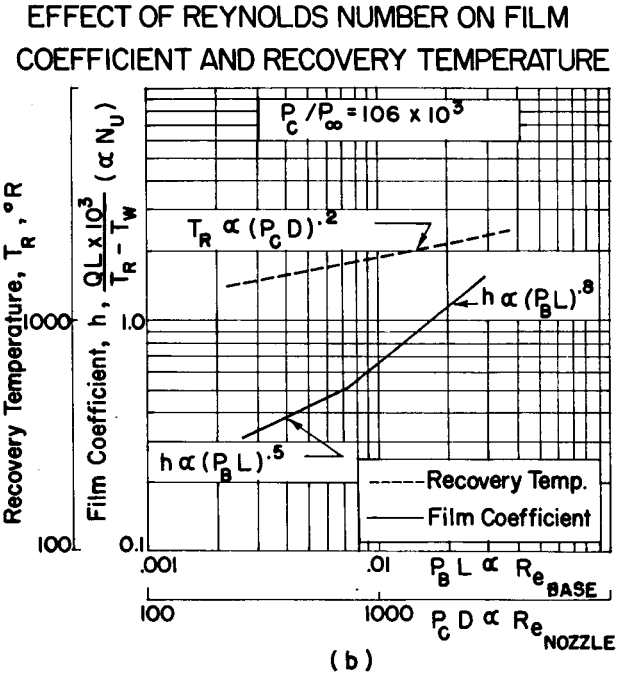

FIGURE 4. DATA OBTAINED WITH SHORT-DURATION TECHNIQUES

the same time provide a facility that would eliminate costly large-scale, wind-tunnel tests. The facility has been developed and has been in operation for about 1 year (Fig. 5). It consists of a tube approximately 4 feet (1.22 m) in diameter and 30 feet (9.14 m) in length in which high pressure gas, 200 psi (1378951.44N/m^2) and lower is stored. A diaphragm retains the gas at the end of the tube. To the right of the diaphragm is the convergent-divergent nozzle which allows the Mach number to be varied. The flow is exhausted into a vacuum tank which is located on the far right of Figure 5.

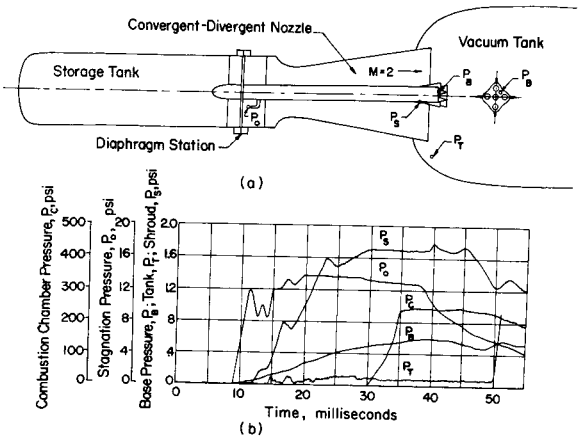

FIGURE 5. SCHEMATIC OF EXTERNAL FLOW FACILITY WITH SOME TYPICAL PRESSURE TRACES

To perform a test, the diaphragm is ruptured and a flow of a certain pressure level and Mach number in the nozzle is obtained for a few milliseconds. About the same time that steady flow is established in the nozzle, the model is fired and the test takes place. Hot and cold flow tests have been made in this facility. Figure 5 also shows typical traces from the early tests at a Mach number of 2.0. P_s is the shroud pressure just ahead of the base; P_o is the stagnation or tube pressure just downstream of the diaphragm; P_c is the combustion chamber pressure within the model; P_b is the typical base pressure trace; and P_t is the pressure within the vacuum tank. The large variation in P_t at approximately 50 milliseconds indicates the return of the blast wave and the end of the test.

The results show that for this length of storage tube approximately 20 milliseconds of constant-flow conditions are available for making tests. Due to the late firing of the combustor, only about 10 milliseconds were used. The storage tube and combustor supply tubes have been lengthened so that considerably longer testing time can be obtained.

Data obtained from the external-flow facility compared reasonably well with large-scale, wind-tunnel tests. The external-flow facility has been built and put into operation for a cost of less than $75,000. By using this facility, some limited Reynolds number effects on base heating were determined. This facility may reduce the number of, or even eliminate, costly wind-tunnel tests for Saturn base-heating studies. A similar, but larger and more versatile facility, has been proposed by MSFC and some feasibility tests for the facility have been made by MSFC.

IV. FLOW-FIELD VISUALIZATION

The flow field results from an increasing altitude and decreasing ambient pressure causing the exhaust jets from the rocket engines in a cluster configuration to expand and to impinge with the other jets in the cluster forming a shock wave. Figure 6a shows a sketch of the flow field. Because of the formation of the shock waves and the resulting pressure rise, a portion of the low-energy, exhaust gases within the boundary layer of the nozzle wall and in the mixing layer around the periphery of the jets will not have sufficient energy to negotiate the pressure rise and will be forced back toward the base plate of the engine. The reverse exhaust gases will then flow radially outward between the nozzles into the atmosphere, or ambient flow, and may choke the engines at sufficiently high altitudes. This condition has caused severe heating on the Polaris and the center star areas of the Saturn vehicles.

Figure 6b is a schlieren photograph of the shock waves formed by the impinging jets. Some results from electron-beam, density measurements on the short-duration, S-IV four-engine model are shown in Figure 6c. The solid lines represent lines of constant density in the form of density ratio (ρ_b/ρ_c) where ρ_b is the ambient density in the reverse flow field and ρ_c is the density within the combustion chamber. The gas is hot nitrogen (2500° R) at a pressure of 200 psi (1378951.44N/m^2). The dashed lines represented the nozzle and the approximate plume impingement. The abscissa is the base radius and the ordinate is the number of inches downstream of the base plate. Starting at the centerline and proceeding toward the base plate, the density decreases which indicates an

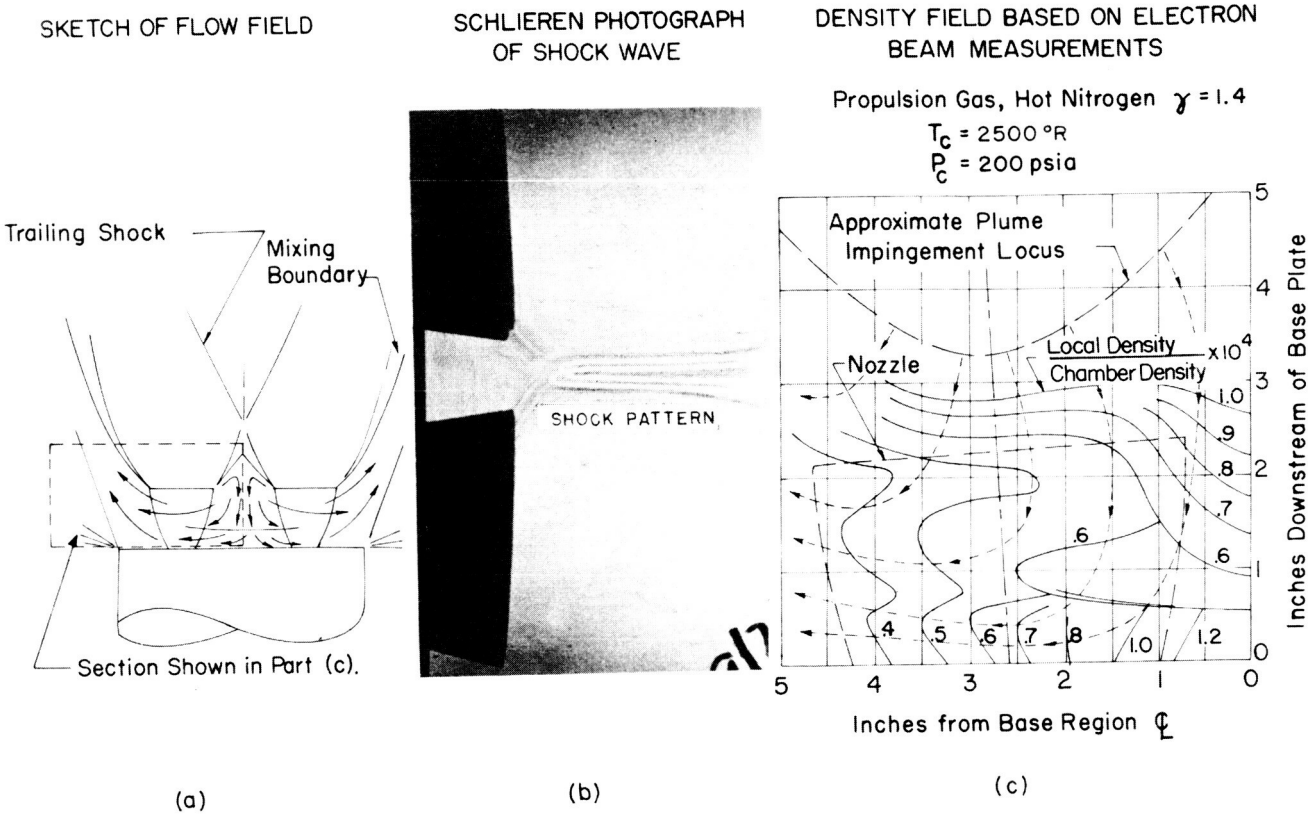

FIGURE 6. RESULTS FROM FLOW-FIELD, VISUALIZATION STUDY

accelerating flow field. A short distance above the base plate, a large increase in density occurs which indicates the presence of a shock wave. Moving farther from the base plate, the density decreases indicating an accelerating flow in that direction. This type of flow field has been studied and verified with conventional-pressure instrumentation.

Only some of the initial results from the electron-beam tests are shown in Figure 6. Hardware has been assembled and an attempt at measuring temperature with the electron beam will be made in the near future.

An instrument for the measurement of local gas velocity using the optical Doppler technique is also under development. The Doppler frequency shift depends on the velocity of the moving particles and on the geometry of the scattering media. If the scattering geometry is fixed, measurement of the Doppler shift gives sufficient information to determine the velocity of the moving particles. This instrument has been built and velocity measurements have been made up to 150 feet per second (45.72 m/s). The instrument is presently being installed in a wind tunnel for measurements of Mach 3 to 5. This technique seems applicable also for gas-turbulence measurements, dynamic-pressure-transducer-calibration, panel flutter studies, and many others.

V. RADIATION

As stated earlier, radiation is the main contribution to base heating for a properly designed LOX-RP first stage. For clustered LOX-H_2 upper-stage configurations, radiation may not be the predominant cause of heating; but it should be accurately computed since the stages fly a long period of time. In order to compute the radiation, the flow-field (velocity, pressure, temperature, composition, etc.), absorption data for radiating components and a radiant program for calculating the intensities must be known. Programs are in existence for calculation of the flow field from a single-engine configuration for frozen or equilibrium flow. Some rough estimates of the flow fields in the impinging regions are currently being used for design purposes. Recently, two programs have been started for computing the flow field for clustered configurations. One is a three-dimensional method of characteristics at Norair and the other is a finite difference scheme at General Dynamics/Convair.

Until some new programs were initiated, the techniques and data available to calculate the radiant heat from H_2O, CO_2, and CO used the total emmissivity data of Hottel measurements during the late twenties and early thirties. These data could not be accurately extended to the range of low pressure, high temperatures, and nonisothermal conditions existing in the fuels of current interest, RL-10, J-2, etc. It is possible to compute some of the data needed with existing high-speed computers, but this is difficult and would require an enormous amount of computing time. Therefore, the "band model" concept was used to describe the absorption coefficient for the radiating components. To use this concept, it is necessary to know such parameters as spectral-line strength, spectral-line spacing, and line half-width. Programs have been initiated and some results have been obtained for some of the band-model parameters needed. Within the next year, it is expected that all parameters needed will be measured so that radiation from present motors can be computable within the accuracy of existing flow fields.

Figure 7 presents some early results of the "band model" concept. The upper part of the curve compares experimental data with "band model" data for water vapor. The results indicate that the "band model" concept is relatively good. The graph in the lower left-hand corner compares the recent emmission data of water vapor of GD/C (Ferriso and Ludwig) with Hottel's results. The results indicate that design data based on Hottel's results would underestimate heating rates. These results are supported by early experimental data. A comparison of the experimental absorption data for carbon with theory (Stull and Plass, modified for index of refraction) is shown in the lower right-hand graph. The results of the experimental absorption data are relatively good except at the lower wavelengths.

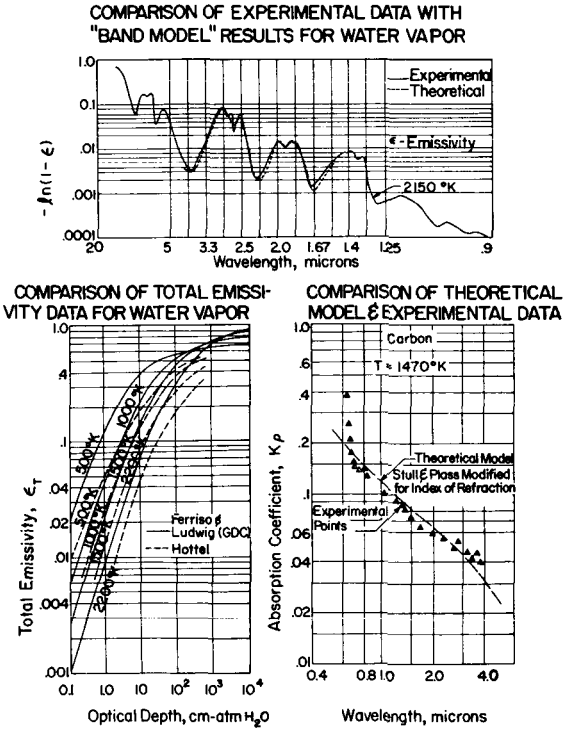

FIGURE 7. COMPARISON OF EXPERIMENTAL DATA WITH "BAND MODEL" RESULTS FOR WATER VAPOR

VI. INVESTIGATION OF COMBUSTION OF HYDROGEN IN A HYPERSONIC AIRSTREAM

Heat leaks to hydrogen-filled fuel tanks made it necessary in some cases to dump combustible hydrogen during flight. Since hydrogen will mix with the ambient air flow, the possibility of it combusting and releasing large amounts of heat in the vicinity of the vehicle has been investigated through a contract with General Applied Sciences Laboratories. Chemical kinetic studies were performed to determine where in the launch trajectory conditions would be favorable for combustion. Fluid mechanical mixing models were set up to investigate two dumping configurations: tangential slot injection, and injection by means of jets located parallel to, but removed from, the surface of the vehicle (Fig. 8). Also more sophisticated flow models employing finite-rate chemistry kinetics were developed.

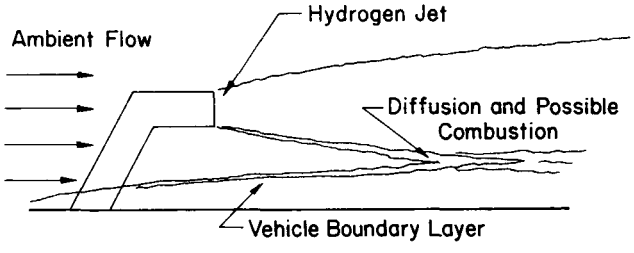

FIGURE 8. MIXING OF HYDROGEN JET WITH VEHICLE BOUNDARY LAYER

To help determine where in the launch trajectory conditions would be most favorable for combustion, two-phase flow phenomenon and the condensation and evaporation associated with the dumping of cryogenetic hydrogen were investigated. The analytical formulations from the above investigation were also supported by experimental investigations of both tangential slot and jet dumping configurations. The results from the above investigations have shown that the hydrogen and air will mix in lengths which are short compared to practical vehicle dimensions and will form mixtures whose composition will fall within

the combustion limits of the air-hydrogen system. If local hot spots are present in the flow field, such as high-static temperature occurring in the boundary layer or increased heating due to protuberances, combustion can be initiated. Combustion may not begin immediately, but may be suppressed because of the high heat capacity of the hydrogen.

The results of the investigation also show that upstream ejection of hydrogen can be accomplished without hazard of ignition or combustion by venting parallel to the surface through a perfectly expanded nozzle if it is displaced far enough from the vehicle to reduce hydrogen levels below flammability limits.

Some results of this program are being used in the Saturn Centaur studies.

RAREFIED-GAS DYNAMICS

By

James O. Ballance

SUMMARY

This study develops two new techniques for the analysis of complicated impact pressure probes at various speed ratios and angles of attack. The first technique is based on the analogy of radiant-heat transfer to that of free-molecular-flow. The second technique uses the Monte Carlo method of selecting random numbers to follow the paths of individual molecules in a system.

The calculation of the drag coefficient of a concave hemispherical shell is extended from the limiting case where all incoming flow is perpendicular to the opening plane of the shell to the case where the incoming flow is at some angle α to the opening plane of the shell.

A modification of the Monte Carlo method is being used in the flow analysis of a cylindrical duct in the transition-flow regime. This method illustrates that a Knudsen number value based only on the diameter of the duct is not sufficient to define the limit for free-molecular-flow but that the length of the duct also has an important effect on the flow.

Thermal-accommodation coefficients have only been measured for low-energy collisions and even then the results are questionable. A program is being conducted to measure the momentum and energy accommodation coefficients up to and exceeding the escape velocities on typical engineering surfaces. The experimental facility used to conduct these measurements is nearly completed, and it is hoped that useful data will be obtained by the end of the year.

I. INTRODUCTION

In the discussion of this topic, it is necessary to establish a reference. The best reference is the mean distance that a gas molecule travels between collisions with other gas molecules (mean-free path). For standard conditions, the mean-free path of an air molecule is approximately 6.6×10^{-8} meters. As the number of molecules per cubic meter (number density decreases, the mean-free path increases. Figure 1 shows the mean-free path for several different values of number density. To obtain a better understanding of the physical significance of these values of mean-free path, the altitudes for the various density levels as given by the United States Standard Atmosphere (1962) are also shown in Figure 1. When the number density is very low, the mean-free path is so large that the collisions between gas molecules can be ignored for most studies involving conventional sized objects. This region is known as the free molecular flow regime. As the number density increases, the mean-free path becomes very small, molecular collisions increase, and the flow approaches the continuum-flow regime. The parameter which describes these regions with reference to the object under study is the Knudsen number (Kn). The Knudsen number is the ratio of the mean-free path to the characteristic dimension of the object. For example, the characteristic dimension of a cylinder is normally taken to be the diameter of the cylinder. Figure 2 shows the flow regimes as normally defined in terms of the Knudsen number.

(US Standard Atmosphere, 1962)

ALTITUDE (kilometer)	NUMBER DENSITY (molecule / m^3)	MEAN FREE PATH (meter)
0	2.55 x 10 + 25	6.6 x 10 - 8
50	2.14 x 10 + 22	7.9 x 10 - 5
100	1.04 x 10 + 19	1.6 x 10 - 1
150	4.10 x 10 + 16	4.0 x 10 + 1
200	7.82 x 10 + 15	2.2 x 10 + 2
250	2.49 x 10 + 15	6.8 x 10 + 2
300	9.50 x 10 + 14	1.8 x 10 + 3
350	4.15 x 10 + 14	4.1 x 10 + 3
400	1.96 x 10 + 14	8.6 x 10 + 3

FIGURE 1. MEAN-FREE PATH OF AIR AT VARIOUS ALTITUDES

KN = KNUDSEN NUMBER

= λ/L WHERE λ = MEAN FREE PATH

L = CHARACTERISTIC DIMENSION

FREE MOLECULAR FLOW	KN > 10
TRANSITION FLOW	10 > KN > 0.1
SLIP FLOW	0.1 > KN

FIGURE 2. FLOW REGIMES FOR RAREFIED-GAS-FLOW

This study is mainly concerned with the free-molecular-flow (Kn > 10) and the near-free-molecular-flow (1 < Kn < 10) portion of the transition-flow regime. This study is grouped into the following four basic types:

(a) Pressure probe characteristics for environmental measuring devices.

(b) Aerodynamic coefficients for orbiting vehicles in both transitional-flow and free-molecule-flow regimes.

(c) Jet spending characteristics for propulsive jets, vent systems, etc., at orbital altitudes.

(d) Surface physics studies for high-velocity, gas-surface interaction.

II. PRESSURE PROBE CHARACTERISTICS

Measurements of density, composition, temperature, and other thermodynamic properties of the upper atmosphere are usually made on a gas that has been brought to rest in a density and composition-sensitive gage connected to the free stream by an orifice or an orifice-restricted tube. The flow parameters that relate the properties in the gage with the free stream are a function of the orifice size, tube length to diameter ratio, energy-accommodation coefficients, relative velocities of the tube and free-stream, thermal motion, angle of attack, etc. Calculated solutions for simple, impact-pressure probes at various speed ratios and angles of attack have been made; but when more complicated geometries are considered, no convenient solutions exist. Two new methods are being used for this analysis which not only yield the desired parameters, but also give better insight into the problems.

The first method uses the analogy of radiant-heat transfer and free-molecular-flow. In free-molecular-flow, an assumption is made that molecules leave a surface element in a direction proportional to the cosine of the angle between the direction vector and the normal to the surface. Also, the molecules are assumed to travel in rectilinear paths between collisions with the surfaces. These assumptions are quite similar to those used in radiant-heat-transfer calculations. Figure 3 compares the molecular flow rate through a duct calculated by this method to the numerical solutions of Clausing [1].

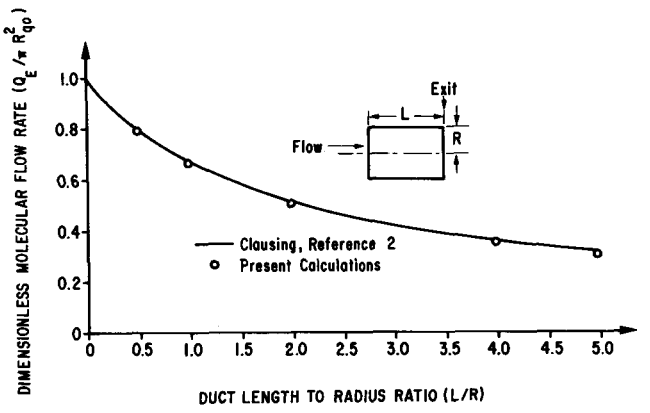

FIGURE 3. MOLECULAR-FLOW RATE THROUGH DUCT AS A FUNCTION OF DUCT LENGTH TO RADIUS RATIO, L/R

A second method uses Monte Carlo techniques where random numbers are used to follow the path of individual molecules through the system. By following a large number of molecules (e.g., 10,000), the properties of the entire system can be determined. Figure 4 shows the transmission probabilities for tubes as a function of speed ratio. The speed ratio is the ratio of gage velocity to the random-thermal speed of the gas molecules. The data in this study are for cases where there is relative motion between the tube and the gas, such as a density gage on a satellite. These data are believed to be the first ever published for orifice-restricted tubes. Figure 5 shows transmission probabilities as a function of the angle of attack. Here the speed ratio (S) is 2 and the length-to-radius ratio of the tube is 4. The lower curve is for the case where radius of the orifice (Ro) is the same as the diameter of the tube (that is, there is no restriction). The upper curve shows the case where Ro is 0.707 of the radius of the tube (R). Also shown in Figure 5 are calculated values for the same case using the techniques developed in "Transmission Probability Determination with

Directed Mass Motion and with Mean Free Path Consideration" [2].

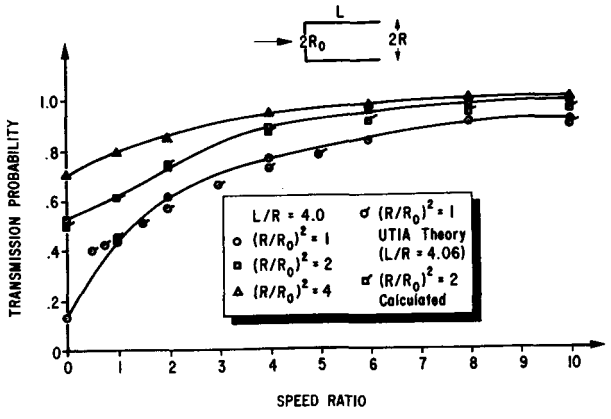

FIGURE 4. TRANSMISSION PROBABILITY FOR TUBES AT ZERO ANGLE OF ATTACK FOR VARIOUS SPEED RATIOS

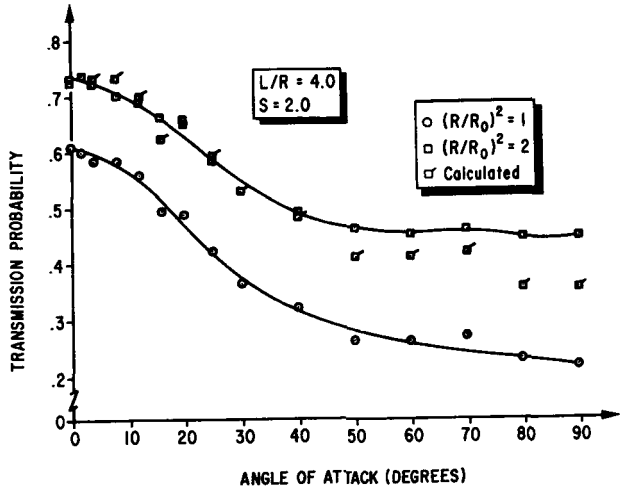

FIGURE 5. TRANSMISSION PROBABILITIES FOR ORIFICE RESTRICTED TUBE AT VARIOUS ANGLES OF ATTACK

III. AERODYNAMIC COEFFICIENTS

Aerodynamic coefficients, such as lift or drag, are easily calculated for free-molecular-flow on simple convex bodies; but when complex or concave bodies are considered, there are no satisfactory solutions. To illustrate the problem involved and to analyze an orbital system, a thorough study of an unusual configuration (the Pegasus satellite) is being made. From this study, more realistic drag coefficients will be generated.

The calculation of the drag coefficient of a concave-hemispherical shell has been extended from the limiting case where all incoming flow is perpendicular to the opening plane of the shell to the case where the flow is at some angle α with respect to the plane of the shell [3]. Figure 6 presents the drag coefficient of a concave hemisphere for speed ratios of 4, 6, and 10 where the temperature ratio of the surface of the hemisphere (T_w) to that of the incident stream (T) is 0.4. Zero angle of attack is when the incoming flow is perpendicular to the plane of the opening of the hemisphere. Using Monte Carlo methods, this effort is being duplicated so that the assumption of hyperthermal flow may be investigated. Hyperthermal flow is that flow which exists when the ratio of the relative speed of an object to the random thermal motion may be ignored, e.g., S = 6. The flow may be considered to be a beam of molecules traveling in parallel paths at a constant velocity. Present theories extend this type of analysis to speed ratios as low as 6.

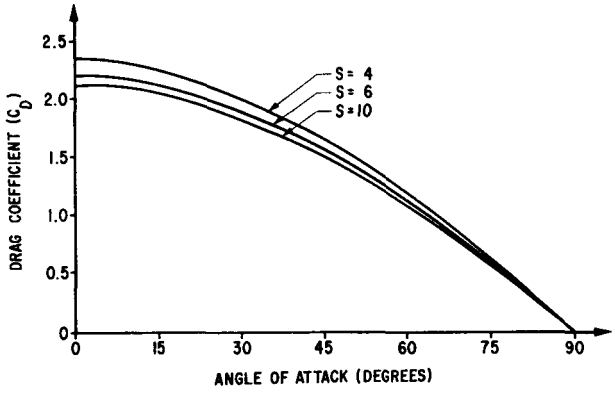

FIGURE 6. DRAG COEFFICIENT, $T_w/T = 0.4$

IV. JET-SPREADING CHARACTERISTICS

The problem of gas impingement of surfaces during low-mass flow or low-density venting has necessitated a closer look at the distribution of flow from tubes. While there is a great deal of information available for the situation where the gas (both in the tube and the free stream) is in the free-molecule-flow condition, little information is available for the case where the gas in the system

is in the transition-flow regime. A modification of the Monte Carlo method is again being used for this study. Figure 7 presents typical data where this modified method was used to study the transition-flow regime in a cylindrical duct. The probability

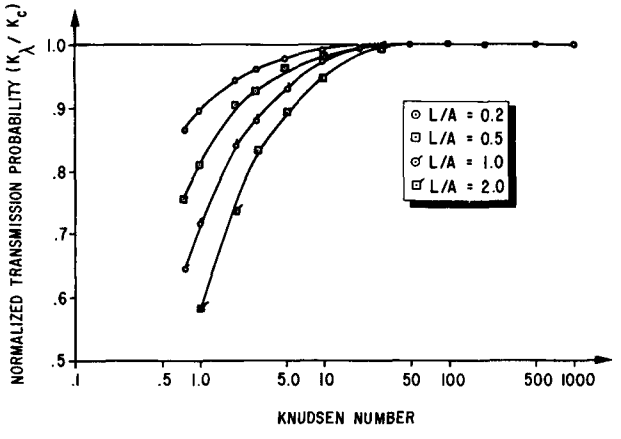

FIGURE 7. NORMALIZED TRANSMISSION PROBABILITIES AS A FUNCTION OF KNUDSEN NUMBERS FOR L/A VALUES OF 0.2, 0.5, 1.0 AND 2.0

(K_c) is the value deduced by Clausing [1] for the case of an infinitely long, mean-free path. The transmission probability (K_λ) is obtained from the modified method for some mean-free path λ. When the ratio K_λ / K_c is equal to 1, the system can be assumed to be in free-molecular-flow. The four curves shown in Figure 7 are for four different length-to-radius ratios (L/A). The curves illustrate that a Knudsen number value based only on the diameter of the duct is not sufficient to define the limit for free-molecular-flow but that the length of the duct also has an important effect on the flow.

V. SURFACE-PHYSICS STUDIES

While the gross effects of studies in rarefied flow are fairly well bounded, they are valid only when consideration is given to the interactions of the gas and the surfaces of the system under study. The microscopic actions in these flows are little known and understood. The parameters that specify these interactions are the reflection and accommodation coefficients. The reflection coefficients are:

$$\sigma = \frac{\tau_i - \tau_r}{\tau_i}$$

$$\sigma' = \frac{P_i - P_r}{P_i - P_s}$$

where

σ = reflection coefficient due to shear stress

σ' = reflection coefficient due to pressures

τ_i = shear stress due to incident mass

τ_r = shear stress due to reflected mass

P_i = pressure due to incoming free-stream-molecules

P_r = pressure due to reflected molecules

P_s = pressure due to reflected molecules at surface temperature

When $\sigma = \sigma' = 0$ specular reflections occur and when $\sigma = \sigma' = 1$ diffuse reflections occur. The thermal accommodation coefficient is:

$$\alpha = \frac{dE_i - dE_r}{dE_i - dE_s}$$

where

dE_i = energy due to incoming free-stream-molecules

dE_r = energy due to reflection molecules

dE_s = energy due to reflection molecules at surface temperature

When α is equal to zero, there is no exchange of energy and when α is equal to one, perfect accommodation takes place. A good method exists for measuring the momentum accommodation of gas molecules on surfaces under study. Thermal-accommodation coefficients have only been measured for low-energy collisions and even then the results are questionable. A program is being conducted to measure the momentum and energy accommodation coefficients up to and exceeding the escape velocities on typical engineering surfaces. The experimental facility is nearly completed, and it is hoped that useful data will be obtained before the end of the year.

VI. EXPERIMENTAL FACILITIES

To verify the limits for the analytical solutions to the problems in this study, it is necessary to perform some experiments. These experiments may be performed in a low-density-research chamber equivalent to that in use by the Aerodynamics Division. This facility is 3.5 ft. (1.07 m) diameter by 14 ft. (4.27 n) in length. A nozzle is being designed to produce a flow of Mach 4. However, it is doubtful that experimental facilities will ever be developed to adequately explore all the problems outlined in this study.

The Aerodynamics Division is conducting a modest program that promises to make a significant contribution in the field of rarefied-gas dynamics.

REFERENCES

1. Clausing, P.: Uber die Stromung sehr verdunnter Gose durch Rohren von beliebiger. Ann Physik 12, 1932, p. 961.

2. Ballance, J. O.: Transmission Probability Determination with Directed Mass Motion and with Mean Free Path Consideration. Third International Vacuum Congress, Stuttgard, Germany, June 1965.

3. Wimberly, C. R.: Determination of Aerodynamic Force and Heat Transfer Properties for a Concave Hemispherical Surface in Free Molecular Flow. NASA TM X-53288, June 1965.

TURBULENT FLUCTUATION MEASUREMENTS WITH THE CROSSED-BEAM METHOD

By

F. R. Krause, M. J. Fisher,* and R. E. Larson**

SUMMARY

A new optical method has been developed for studying aspects of launch-vehicle turbulence. The heart of the method is a new test arrangement for the remote sensing of local changes in radiative power. Early experimental results are given and show that most statistical turbulence parameters can be approximated which are commonly derived from "two point product mean values." The measurement of local thermodynamics' properties in turbulent flows becomes conceivable.

I. INTRODUCTION

The measurement of turbulent fluctuations in the environment of launch vehicles is necessary to provide the input for the statistical analysis of responses like rigid-body motions, elastic deformations, as well as heat transfer and acoustical loads. Solid probes introduce stabilizing walls and/or additional shock waves which interfere severely with the fluctuations of interest. A further instrumentation problem is to find probes with a sufficiently high resolution in space and time so the fluctuations are not integrated out. So far, all ground tests and flight instrumentation are restricted to pressure transducers, thin film gages, and accelerometers that are flush mounted in the vehicle surface. Fluctuation measurements in the flow have not proved to be feasible.

The required inputs or aerodynamic-forcing functions are mathematically similar insofar as they should be expressed by an area integral over a space-time correlation function. The inherent numerical integration requires a large number of points and the experimental and numerical effort in providing these pointwise estimates is almost prohibitive, even if a large number of transducers are used in the vehicle walls. Therefore, this study proposes to use the integrating features of optical beams for a "one shot" estimate of area-integrated-correlation functions in the flow.

* IIT Research Institute

** Applied Science Division, Litton Industries

II. OPTICAL INTEGRATION OVER CROSS-CORRELATION AREAS

Statistical thermodynamics show that the light extinction coefficient μ is determined by the thermodynamic properties of the flow [1]. Therefore, its space-time correlation might be used to study the turbulent fluctuations of thermodynamic flow properties.

Consider the experimental arrangement in Figure 1. Two narrow beams of white light traverse a jet in the y and z directions. Using an optical filter in front of the photo detectors, the received radiative power is limited to the wavelength interval $\Delta\lambda$ centered around the wavelength λ. The intensity fluctuations of the y and z beams are now correlated and normalized with the mean values. These operations lead to the measurable quantity

$$G(\xi,\tau)_x = \frac{\langle i_z(t)\, i_y(t+\tau)\rangle}{\langle I_y\rangle \cdot \langle I_z\rangle} \qquad (1)$$

Fisher and Krause [2] show analytically that the measurable quantity is related to the two-point, product-mean value of the light extinction coefficient

$$R\mu(\xi,\tau)_x = \qquad (2)$$

$$\overline{\langle \mu'(s, y, z, t)\mu'(x+\xi, y+\eta, z+\zeta, t+\tau)\rangle}$$

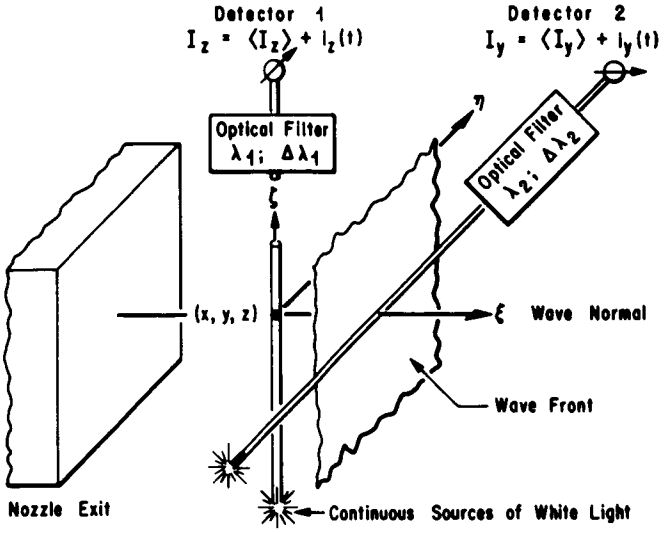

The crossed beam technique gives the integrated cross correlation function of light extinction coefficients.

$$\frac{\langle i_z(t)\, i_y(t+\tau)\rangle}{\langle I_z\rangle \quad \langle I_y\rangle} = G(\xi,\tau) = \iint_{-\infty}^{+\infty} R_\mu(\vec{\xi},\tau)\, d\eta\, d\zeta$$

$$R_\mu(\vec{\xi},\tau)_{\vec{x}} = \langle \mu'(\vec{x},t)\, \mu'(\vec{x}+\vec{\xi},t+\tau)\rangle$$

$$\mu(\vec{x},t,\lambda,\Delta\lambda) = \frac{\text{Filtered power loss along } \Delta Z}{\text{Filtered energy flux} \cdot \Delta Z \cdot \Delta X}$$

FIGURE 1. OPTICAL INTEGRATION OVER WAVE FRONTS IN TURBULENT FLOWS

by an area integration across the plane in which the beams have been aligned.

$$G(\xi,\tau)_x = \int_{-}^{+} \int_{\infty}^{\infty} R_\mu(\xi,\tau)_x \, d\eta\, d\zeta \ . \qquad (3)$$

The derivation of equation (3) shows that the wanted "one shot" estimate of area integrated correlation functions can be obtained, even in statistically inhomogeneous media, as long as there is one direction of homogeneity left. The wavelength λ and the spectroscopic resolution $\Delta\lambda$ may be adjusted to a specific thermodynamic property, such as density, species concentrations, and, hopefully, temperatures.

III. APPROXIMATION OF POINT MEASUREMENTS

The random nature of turbulent fluctuations assures that the integrand in equation (3) drops to zero over finite and mostly small distances. In this fashion, local information can be obtained that depends on the turbulence structure. To be more specific, assume that the dependence of R_μ on the beam separation ξ and the time separation τ might be approximated through a separation of variables. Within the validity of this assumption, all turbulence parameters can be obtained which are commonly derived from two point product mean values [3]. This is demonstrated in graphical rather than mathematical form.

The integral scale of turbulence follows from the space correlation as shown in Figure 2. It is equal to that separation distance which makes the cross-hatched areas equally big. The integral scale depends on the direction of the beam separation. The subscript x denotes a separation in the streamwise direction. If the beam separation is repeated along the remaining perpendicular y and z axis, the values L_y and L_z could be obtained. These values are used to calculate mean-square values from the measurements at zero-beam separation.

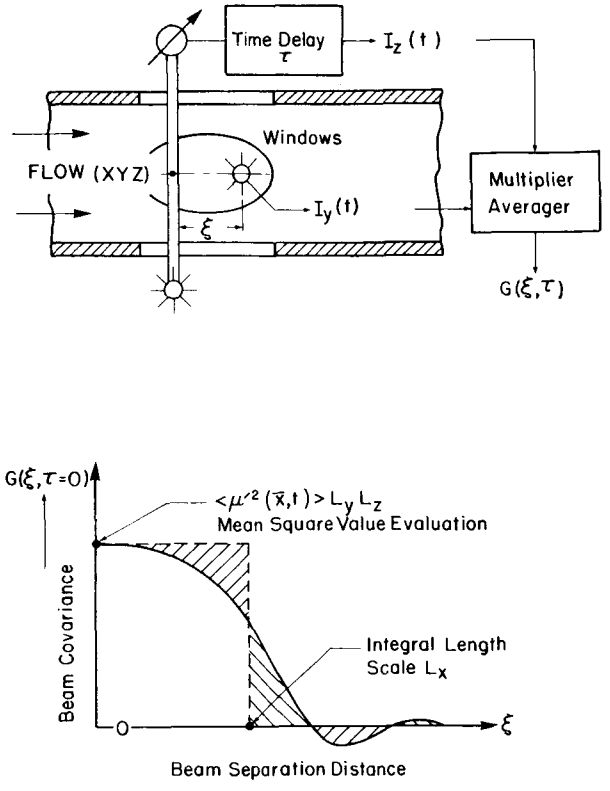

FIGURE 2. TURBULENCE SCALES AND INTENSITIES FROM CROSSED-BEAM COVARIANCE MEASUREMENTS

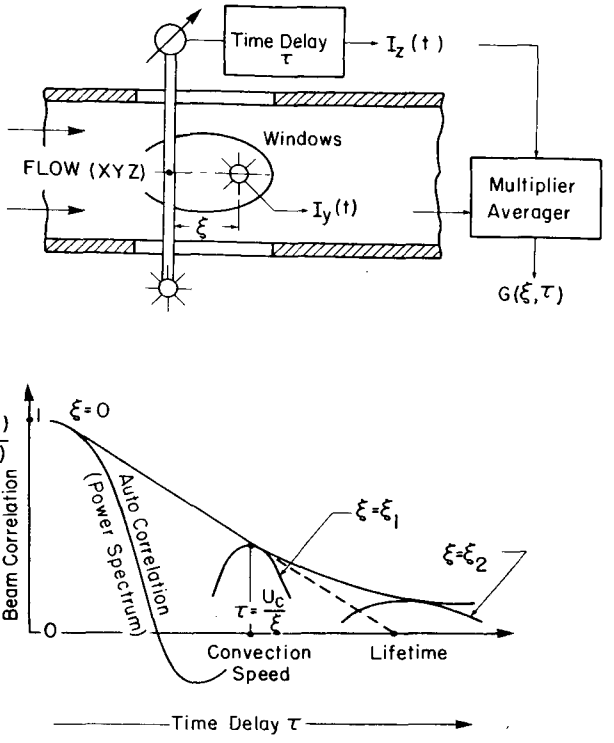

FIGURE 3. LOCAL POWER SPECTRA CONVECTION SPEEDS AND EDDY LIFETIMES FROM CROSSED-BEAM CORRELATION MEASUREMENTS

Using the existing computer programs [4] for random vibration analysis, a time log can be introduced between the records of the two photo-detector outputs. Plotting the calculated G values against this time separation instead of space separation gives additional turbulence parameters as shown in Figure 3. For zero space separation, the measured, temperature-correlation function resembles the auto correlation and can be used to calculate the shape of the power spectrum. Plotting the temporal correlation function $G(\tau)\xi$ for one constant space separation enables the bulk convection speed U_c to be read from the time lag corresponding to the first maximum correlation. Repeating this plot for several beam separations gives an envelope which indicates the eddy-lift time.

The pointwise estimates are only approximately correct because of the assumed separation of variables. The case, which is not covered, occurs when the separation of variables is erroneous for turbulent fields with large scales. Large lateral scales now indicate that only relatively few wave-number components are involved in the turbulent exchange. Separation of variables assumes that the lateral-wave-number components do not interact. Thus, the case not covered would demand a strong interaction between a few lateral-wave-number components which are not communicated to other regions of the wave-number space. Such a process will be broken up by the action of the nonlinear terms in the equations of motion. Therefore, the crossed-beam methods should give a good approximation of point measurements in almost all turbulent fields of practical interest.

IV. EXPERIMENTAL RESULTS

The most revealing and instructive test of the crossed-beam concept is to compare the optical approximation of point measurements with known hot-wire measurements. All measurements were taken in a subsonic (M=0.2) air jet exhausting through a 1-inch (2.5 cm) diameter nozzle into the atmosphere (Fig. 4). Light extinction was achieved by spraying a small amount of liquid nitrogen into the settling

chamber. This produces small water droplets in the exhaust flow which attenuate the crossed beams by scattering.

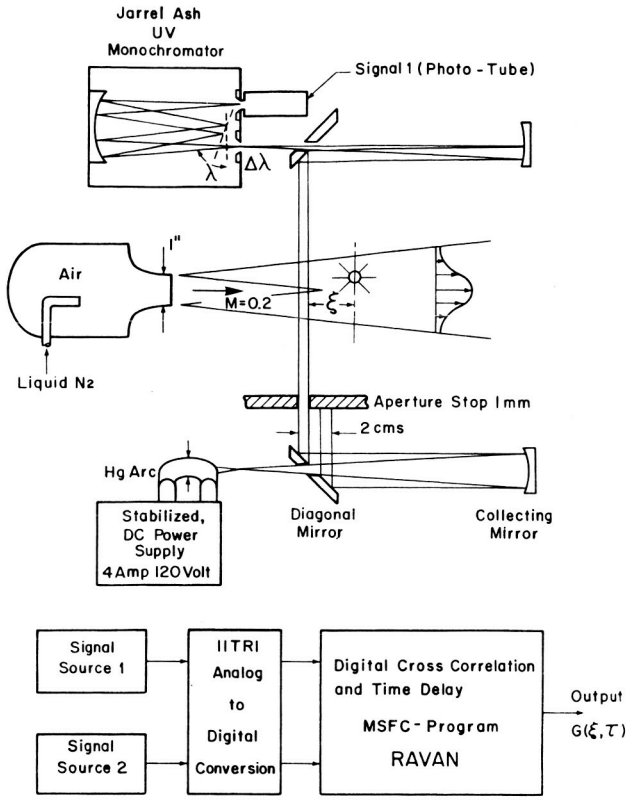

FIGURE 4. THE FIRST CROSSED-BEAM CORRELATOR

A diagram of the optical and electronic hardware is shown in Figure 4. A plane and a spherical mirror collects the light from a powerful mercury arc and transmits it as a parallel beam through the jet. A similar mirror combination projects the arc image on the entrance slit of a grating spectrograph. The aperture stop in front of the spectrograph is set at a beam diameter of 1 mm. The photo-multiplier then scans the first order spectrum of the grating. In this way, the wavelength interval $\Delta\lambda$ and the wavelength λ are adjusted by the width of the monochromator slit and the rotation of the grating respectively. By exchanging light sources, gratings, and photo detectors, the system is able to cover the spectrum from the vacuum ultraviolet (λ = 1200A) to the infrared ($\lambda = 25\mu$).

The above light source and detector arrangement is used to generate two beams, one in a horizontal direction and one in a vertical direction (Fig. 5).

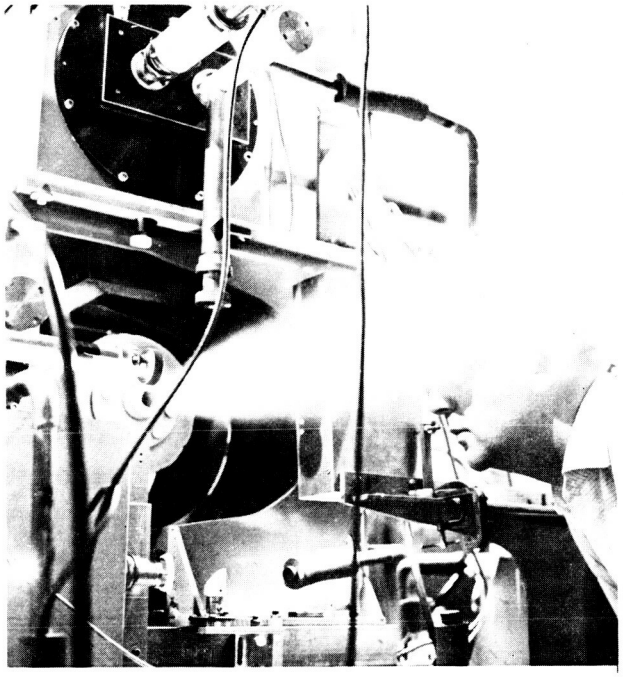

FIGURE 5. LIGHT SOURCE AND DETECTOR ARRANGEMENT

A lathe bed provides a mechanical support which allows the beams to be aligned parallel to the nozzle-exit plane. A beam separation in the streamwise direction gives longitudinal turbulence scales and convection speeds. Transport of the whole system allows us to repeat the measurements for all axial and radial traverses of the jet. However, beam orientation at an angle to the nozzle-exit plane is not possible and the associated-lateral scales have not yet been measured.

The contribution of correlated, light-source fluctuation, created by power supply main ripple, was eliminated using electronic filters. Figure 6 shows measured, temporal, cross correlation for various streamwise beam separations that were taken along the center of the shear layer 3 diameters downstream from the nozzle exit. Each curve is normalized by the maximum value of the correlation coefficient observed at that particular separation. This form of presentation was necessitated by a certain inconsistency of peak values which are not fully understood. However, the peaks of the various curves presented clearly indicate the presence of a convected, turbulent pattern. Plotting the known space separation against the time lags that are indicated by the maximum temporal correlation function results in a line. The slope of this line indicates the convection speed as discussed previously.

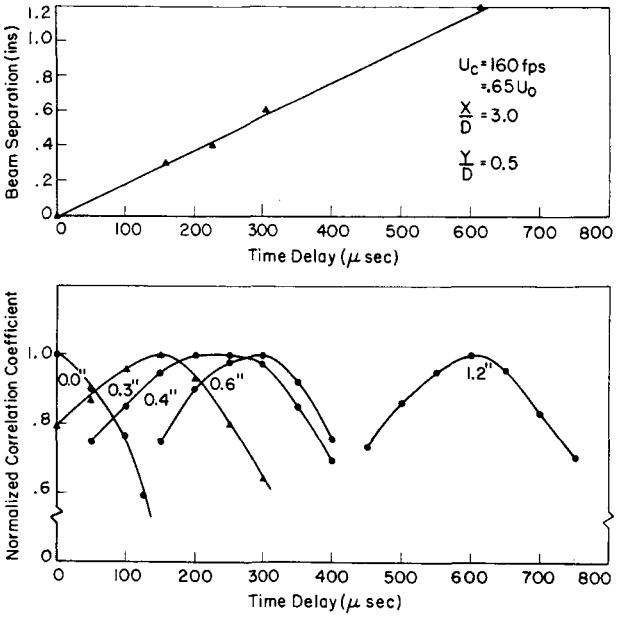

FIGURE 6. CONVECTION VELOCITY FROM CROSSED-BEAM CORRELATION

Figure 7 shows the temporal, cross-correlation results. The only difference from the previous results is that the beam interaction point has been moved radially outwards by 0.2 inch (0.51 cm). These figures yield two points on the convection speed profile which is established from the hot-wire measurements of Davis and Fisher [5] as shown in Figure 8. The difference between the crossed-beam measurements and the hot-wire measurements fall within the scatter of the hot-wire points. The spatial resolution of the crossed beam is good considering that the two measurements were only 0.2 inches (0.51 cm) apart.

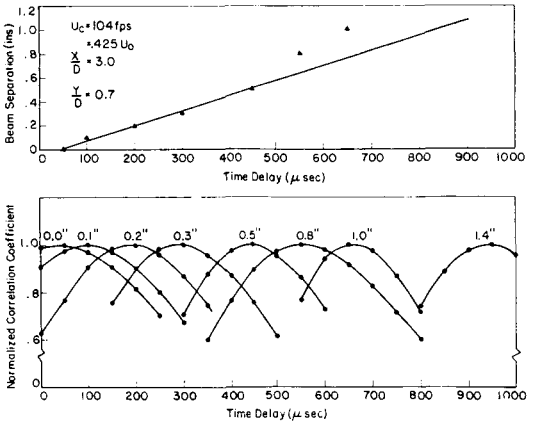

FIGURE 7. CONVECTION VELOCITY FROM CROSSED-BEAM CORRELATION

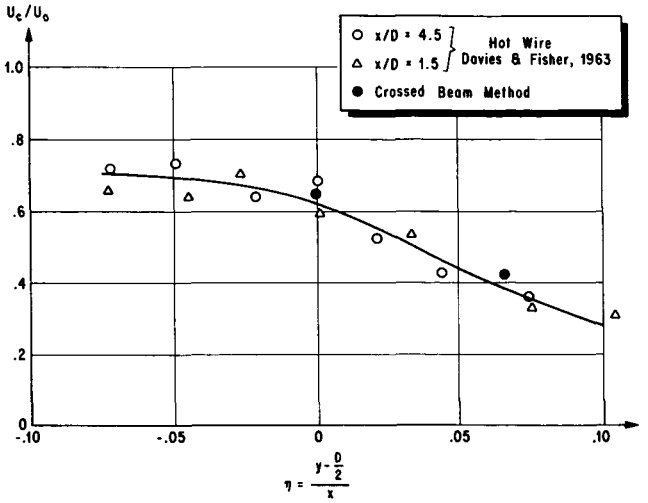

FIGURE 8. COMPARISON OF RADIAL DISTRIBUTION OF CONVECTION VELOCITY

The comparison between the optically determined space-correlations and the hot-wire results of Laurence [6] and Bradshaw [7] are shown in Figure 9. The optical results fall in between the hot-wire

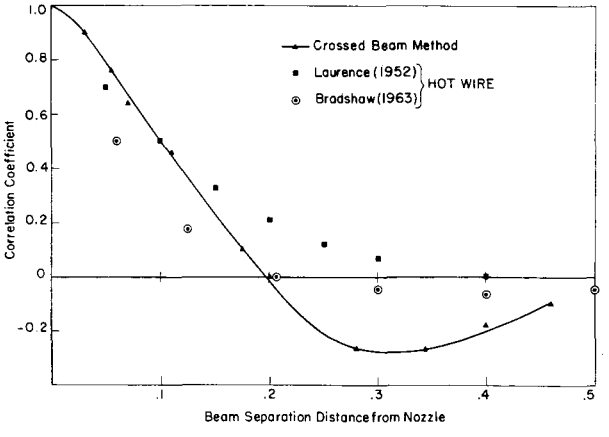

FIGURE 9. MEASUREMENT OF EDDY SCALES

results. Once again, this good comparison is very encouraging. At larger space separations, the crossed-beam method indicates considerable negative space-correlation, whereas the hot-wire correlations have decayed to almost zero. Many of Laurence's auto-correlation measurements and Bradshaw's space correlations also show a negative loop, but its amplitude is generally less than that indicated by the crossed-beam method.

The discrepancies at the large space separations could be explained by errors in either the hot-wire or the crossed-beam method. The hot wire is subjected to all velocity components; and at large separations, the transverse-velocity fluctuations could add so much noise that the correlation disappears. The crossed-beam method could provide erroneous results if the water droplets follow only the large-scale eddies. These eddies are limited to a range of small wave numbers which show a large correlation that disappears when all wave numbers are considered.

Figure 10 shows an initial measurement of the radial intensity profile of concentration fluctuations.

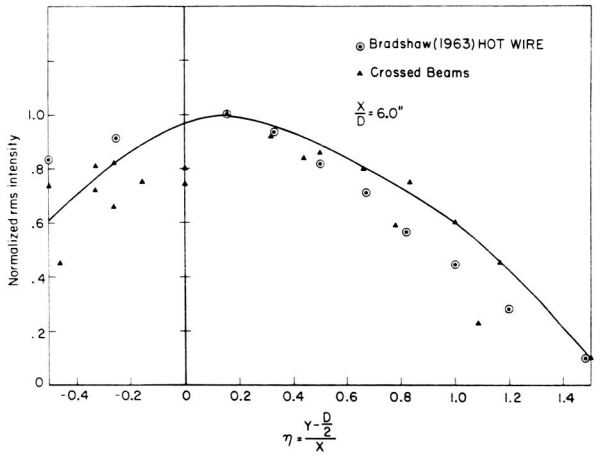

FIGURE 10. TURBULENT INTENSITY PROFILES

For this measurement, the beams were arranged to intersect in a plane 6 diameters downstream of the exit. The vertical beam was moved to various positions across the flow, thereby changing the radial location of the intersection point. For each radial separation, the rms amplitude was evaluated following the procedure that was already described in Figure 2. Since lateral scales cannot be measured with the present support, it was assumed to be equal to the longitudinal scale. In spite of this simplification, the agreement with the hot-wire results from Bradshaw are again very encouraging.

The crossed-beam results in Figure 10 are scattered. Any one determination shows a comparatively smooth variation of intensity and the peak value occuring close to the center of the shear layer as expected. However, the decrease on either side of the maximum varied in repeated runs. Since the runs were performed on days when the external relative humidity was very different, it is suspected that the water vapor content of the air delivered by the jet modified appreciably the degree of persistence of water droplets in the flow. Thus, it is tentatively concluded that the scattering of the results is a real effect associated with a lack of control in the introduction of the water droplet content rather than in the limitation of the crossed-beam method.

V. FUTURE APPLICATIONS

The first contribution to the Saturn program will be to measure turbulence shock-wave interaction in the plume impingement and recirculation areas of the S-IC and S-II rocket clusters. Model tests at MSFC's impulse base flow facility indicated extremely high fluctuations of wall pressures and heat-transfer rates as shown in Figure 11. These fluctuations create

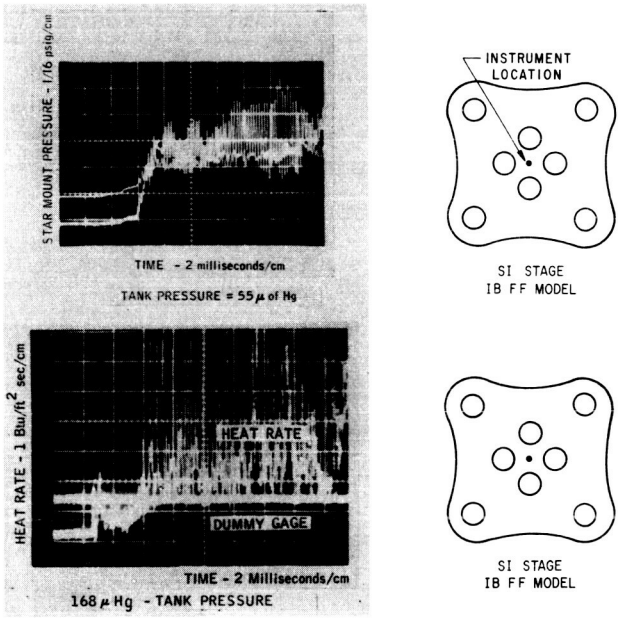

FIGURE 11. TURBULENT FLUCTUATIONS OF BASE PRESSURE AND HEAT TRANSFER RATES

problems when predicting heat-transfer rates. Turbulence levels of only 3 percent have sometimes increased the stagnation point heat transfer on cylinders up to 80 percent. Hot-wire measurements on the two-dimensional-base-flow model already indicate turbulence levels in excess of 100 percent as shown in Figure 12. Therefore, the turbulence effects on heat transfer might play a dominant role. They could increase or decrease the heat transfer by either transporting the hot particles into the wall layers or

throwing them back from the wall. These effects cannot be included in the present model tests on analytical solutions. Therefore, the crossed-beam method is needed to study the turbulent heat and mass transport in base flows.

Other optical fluctuation measurements in clustered rocket exhausts are necessary to predict and/or prevent high acoustical loads on the upper stages. The presence of powerful Mach-wave and shock-wave sound radiation is shown on the shadowgraph in Figure 13. In the case of single jet, the sound radiations are not so dangerous, since they are directed away from the vehicle. However, on a rocket cluster, the sound radiation can pass through the subsonic hole between the plume impingment shocks and will then hit the vehicle directly. The presence of such a subsonic hole and the oscillation of the plume impingement shock are clearly indicated on the schlieren and interferograms of our two-dimensional-base-flow model (Fig. 14). The associated, aerodynamic, feedback loops will produce a jet noise problem on the upper stages, as soon as plume impingement and a choked-flow establish a finite base pressure. For the S-II stage, a conservative estimate of sound pressures is 153 dB.

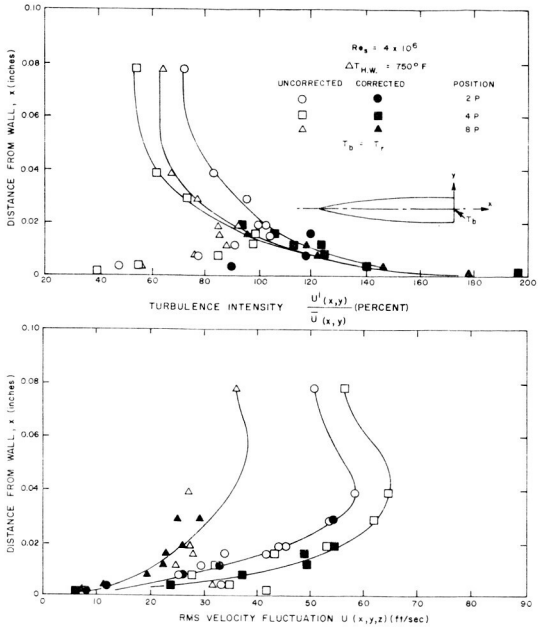

FIGURE 12. RMS VELOCITY PROFILES IN TWO-DIMENSIONAL-BASE FLOW WITH AND WITHOUT WALL EFFECT

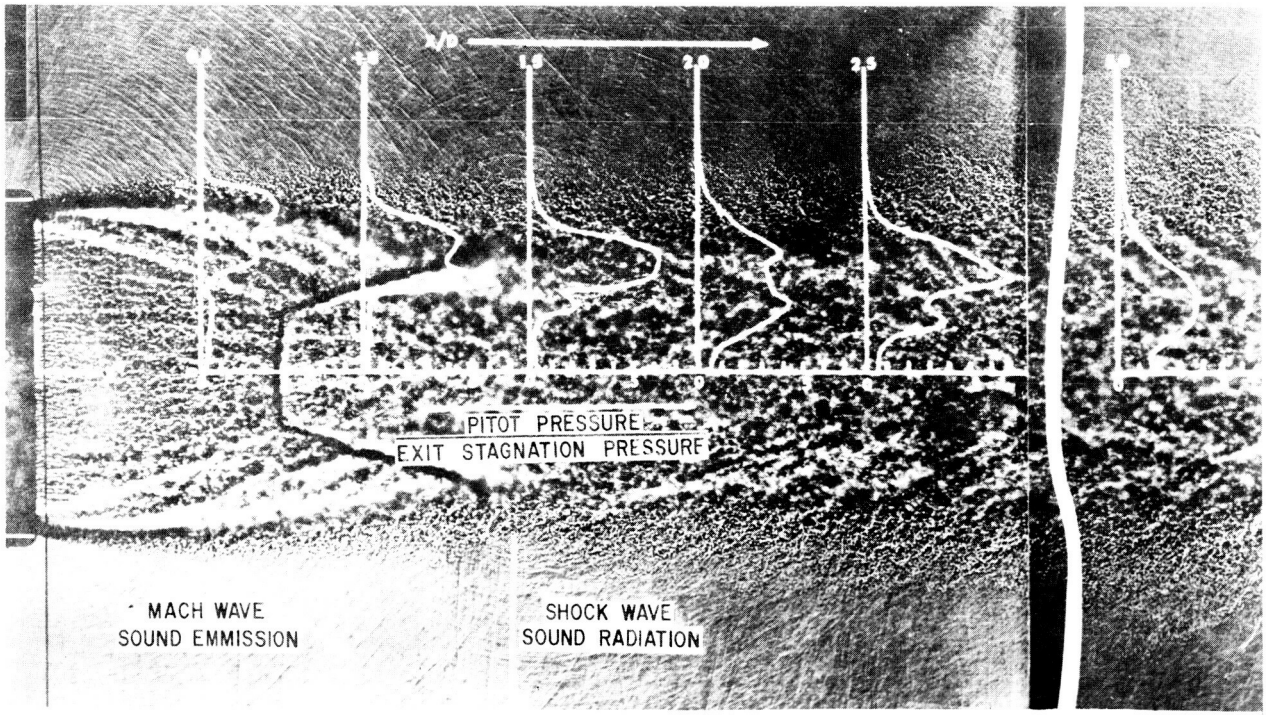

FIGURE 13. SUPERSONIC NOISE SOURCES IN A SINGLE F-1 ENGINE JET

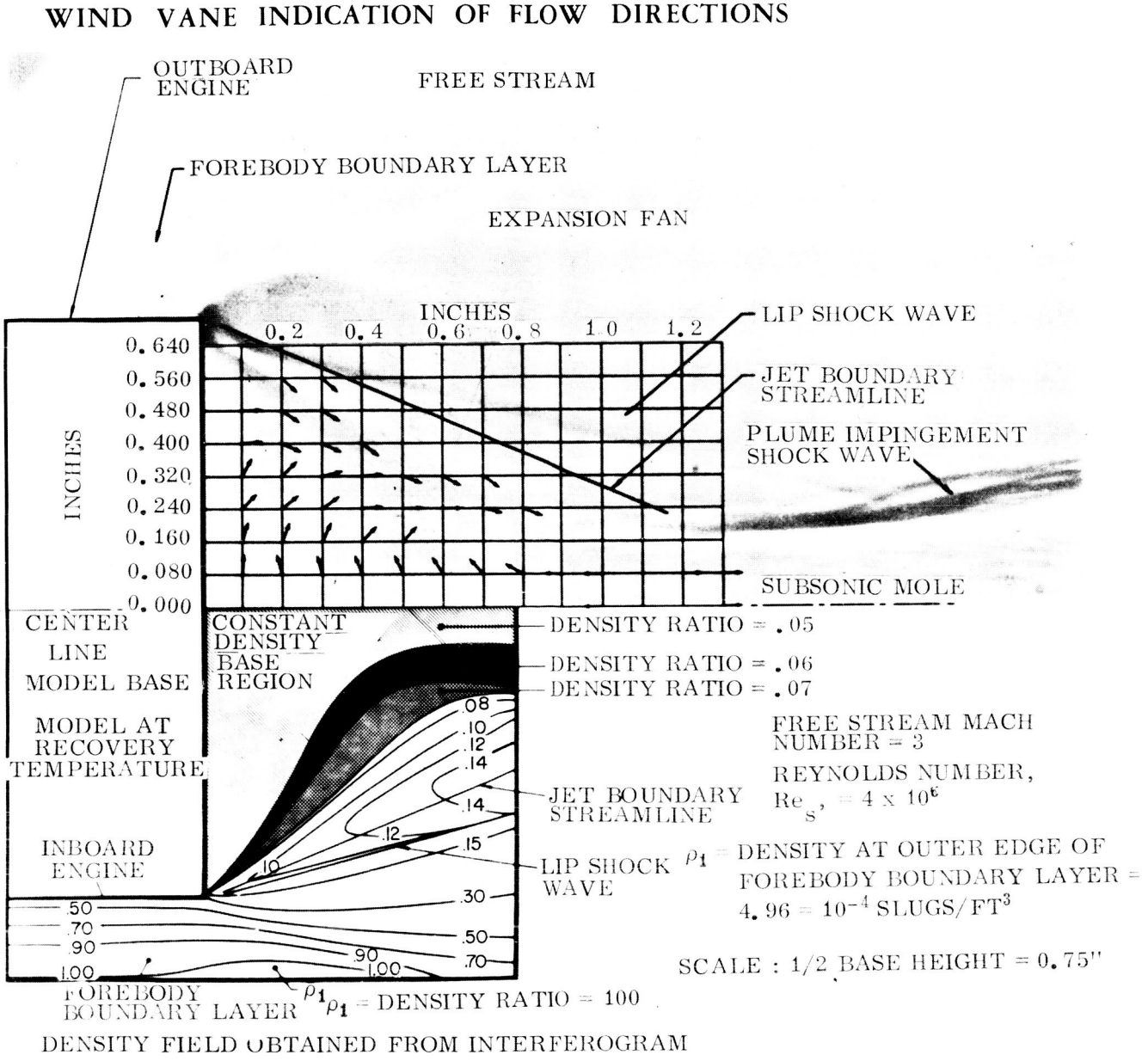

FIGURE 14. RECIRCULATION ZONE FLOW FIELD

The use of laser beams, if feasible, would allow crossed-beam measurements over vast areas. Speculations could also be made about water vapor, carbon dioxide, and ozone concentrations in the lower and upper atmosphere. A study of intense-radiation belts is conceivable which use only detectors and no light sources.

If the crossed-beam method works on both particle scattering and gaseous absorption, it could be used on two-phase flows. Fuel mixing in combustion chambers, fuel droplets, and ion particles in liquid and solid rocket exhausts, gas bubbles, and condensation in tanks, etc., are some of the applications that might be of great interest to other laboratories.

The present development of technique is aimed at the oxygen absorption in the untraviolent because of the importance of air flows. The insufficient storage capacity of the computer memory is the only limitation to getting accurate cross-correlation

estimates. However, a new computer program will eliminate this difficulty.

VI. CONCLUSIONS

Local fluctuation measurements through a space and time correlation of optical signals have been successful in a small subsonic jet where the light extinction was produced by scattering at water droplets. Comparing the hot-wire data with the crossed-beam data lead to the following conclusions:

(a) Probe interference and cancellation problems were avoided.

(b) One shot estimates of area integrated correlation functions can be made.

(c) Approximations can be made on the local power spectra, convection speeds, turbulence scales, and eddy lifetimes.

(d) The crossed-beam method can work with existing random vibration computer programs.

An extension that includes light extinction by gaseous absorption and/or emission would show the following potential:

(1) The adjustment to special theromodynamic properties, such as species concentrations by a proper selection of optical wave length and wavelength interval.

(2) Two phase-flow applications by independent measurement of droplet scattering and gaseous absorption.

(3) The measurement of combustion instability and plasma instability.

(4) The location and intensity of atmospheric concentration fluctuations and radiation belts.

REFERENCES

1. Chapman, S.; and Cowling, T. G.: The Mathematical Theories of Non-Uniform Gases. Second edition, Cambridge, 1960.

2. Fisher, M. J.; and Krause, F. R.: Local Measurements in Turbulent Flows Through Cross-Correlation of Optical Signals. Aero-Astrodynamics Research Review Number 2, NASA TM-X-53295, April 1965.

3. Hinze, J. O.: Turbulence. New York, N. Y., 1959.

4. NASA, MSFC, The Vibration Manual. (first edition) 1964.

5. Davis, P. O. A. L.; Fisher, M. J.; and Barrett, M. J.: The Characteristics of the Turbulence in the Mixing Region of a Round Jet. J. Fluid Mech., vol. 15, 1963, p. 337.

6. Lawrence, J. C.: Intensity, Scale and Spectra of Turbulence in the Mixing Region of a Free Subsonic Jet. NACA Rept. No. 1292, 1956.

7. Bradshow, P.; Ferriss, D. H.; and Johnson, R. F.: Turbulence in the Noise-Producing Region of a Circular Jet. Advisory Group for Aeronautical Research and Development, Report 450, Apr. 1963.

RESEARCH ACHIEVEMENTS REVIEW SERIES NO. 12

Aerodynamics Research at MSFC

By

Werner Dahm, M. F. Platzer, Homer Wilson, James O. Ballance,
F. R. Krause, M. J. Fisher and R. E. Larson

The information is this report has been reviewed for security classification. Review of any information concerning Department of Defense or Atomic Energy Commission programs has been made by the MSFC Security Classification Officer. This report, in its entirety, has been determined to be unclassified.

This document has also been reviewed and approved for technical accuracy.

E. D. GEISSLER
Director, Aero-Astrodynamics Laboratory

MSFC INTERNAL

DIR	1
DEP-T	1
DEP-A	1
AST-P	1
CC	1
CC-P	1
LR	1
MA-S	1
PA	2
E-DIR	6
F& D-CH	1
R-DIR	3
R-S	1
R-TS	1
R-AS	5
R-AERO (Through Branch Level)	30
R-AERO-T	9
R-ASTR	25
R-EO-R (Reserve)	50
R-COMP (Through Branch Level)	10
R-COMP-T	5
R-ME (Through Branch Level)	21
R-RP (Through Branch Level)	8
R-P& VE (Through Branch Level)	79
R-QUAL (Through Branch Level)	26
R-QUAL-T	8
R-TEST (Through Branch Level)	12
R-EO-DIR	
Dr. Johnson	1

MSFC INTERNAL (Cont'd)

LVO	2
I-DIR	1
I-I/IB-MGR (Through Branch Level)	10
I-V-MGR (Through Branch Level)	10
I-E-MGR	3
I-MICH-MGR	20
I-MT-MGR	2
MS-T	25
MS-IP	2
MS-IL	8
MS-I, Daniel Wise	1
Air Force Space Systems Division Huntsville, Alabama	1

NASA HEADQUARTERS

Dr. Mac C. Adams, Code R, Washington, D. C.	1
Mr. Milton B. Ames, Jr., Code RV, Washington, D. C.	1
Mr. Walter Beckwith, Code MTP, Washington, D. C.	1
Dr. Raymond L. Bisplinghoff, Code A, Washington, D. C.	1
Mr. Edmond C. Buckley, Code T, Washington, D. C.	1
Mr. Oliver Bungardner, Code MLT, Washington, D. C.	1
Mr. Roland H. Chase, Code RET, Washington, D. C.	1
Mr. Fred J. DeMeritte, Code RV-1, Washington, D. C.	1
Mr. Robert W. Dunning, Code RBA, Washington, D. C.	1
Dr. James B. Edson, Code R-1, Washington, D. C.	1
Mr. Albert J. Evans, Code RA, Washington, D. C.	1
Mr. Harold B. Finger, Code RN, Washington, D. C.	1
Mr. W. Foster, Code SM, Washington, D. C.	1
Mr. Robert Freitag, Code MC, Washington, D. C.	1
Mr. Edward Z. Gray, Code MT, Washington, D. C.	1
Dr. John Holloway, Code SC, Washington, D. C.	1
Maj. Gen. David M. Jones, Code MD-P, Washington, D. C.	1
Dr. Walton L. Jones, Code RB, Washington, D. C.	1
Dr. Hermann H. Kurzweg, Code RR, Washington, D. C.	1
Mr. William E. Lilly, Code MP, Washington, D. C.	1
Dr. Douglas R. Lord, Code MTS, Washington, D. C.	1
Mr. Ivan Mason, Code MAT, Washington, D. C.	1
Dr. George E. Mueller, Code M, Washington, D. C.	1

NASA HEADQUARTERS (Cont'd)

Mr. Joseph L. Murphy, Code KR, Washington, D. C.	1
Mr. Boyd C. Myers, Code RD, Washington, D. C.	1
Dr. J. Naugle, Code SG, Washington, D. C.	1
Dr. Homer E. Newell, Code S, Washington, D. C.	1
Mr. E. O. Pearson, Jr., Code RV-1, Washington, D. C.	1
Maj. Gen. Samuel C. Phillips, Code MA, Washington, D. C.	1
Mr. Maurice J. Raffersperger, Code MTE, Washington, D. C.	1
Mr. Melvin G. Rosche, Code RV-2, Washington, D. C.	1
Mr. Charles T. D'Aiutolo, Code RV-1, Washington, D. C.	1
Mr. J. Warren Keller, Code RV-1, Washington, D. C.	1
Mr. J. L. Sloop, Code RC, Washington, D. C.	1
Mr. S. M. Smolensky, Code MCD, Washington, D. C.	1
Mr. Frank J. Sullivan, Code RE, Washington, D. C.	1
Mr. William B. Taylor, Code MT, Washington, D. C.	1
Dr. M. Tepper, Code SF, Washington, D. C.	1
Mr. Adelbert Tischler, Code RP, Washington, D. C.	1
Mr. Theofolus Tsacoumis, Code RET, Washington, D. C.	1
Mr. Gene A. Vacca, Code REI, Washington, D. C.	1
Dr. John M. Walker, Code RET, Washington, D. C.	1

CENTERS

Mr. H. Julian Allen, Director NASA, Ames Research Center Moffett Field, California 94035	2
Dr. Kurt H. Debus, Director NASA, John F. Kennedy Space Center Kennedy Space Center, Florida 32899	2
Mr. Paul F. Bikle, Director NASA, Flight Research Center P. O. Box 273 Edwards, California 93523	2
Dr. John Clark, Acting Director NASA, Goddard Space Flight Center Greenbelt, Maryland 20771	1
Dr. William H. Pickering, Director NASA, Jet Propulsion Laboratory 4800 Oak Grove Drive Pasadena, California 91103	2
Dr. Floyd L. Thompson, Director NASA, Langley Research Center Langley Station Hampton, Virginia 23365	2

CENTERS (Cont'd)

Dr. Abe Silverstein, Director NASA, Lewis Research Center 21000 Brookpark Road Cleveland, Ohio 44135	2
Mr. Warren Gillespie Code EA 5 NASA, Manned Spacecraft Center Houston, Texas 77001	15
Mr. J. P. Claybourne, EDV-4 Chief, Future Studies Office NASA, John F. Kennedy Space Center Kennedy Space Center, Florida 32899	1
Dr. Winston E. Kock NASA, Electronics Research Center 575 Technology Square Cambridge, Massachusetts 02139	2
Mr. A. R. Lawrence Management Analysis NASA, Electronics Research Center 575 Technology Square Cambridge, Massachusetts 02139	25
Mr. John Boyd, Technical Assistant Office of Assistant Director for Astronautics NASA, Ames Research Center Moffett Field, California 94035	1
Mr. Chesley H. Looney, Jr., Ass't Chief Advanced Development Division NASA, Goddard Space Flight Center Greenbelt, Maryland 20771	1
Mr. James F. Connors, Chief Office of Research Plans and Programs NASA, Lewis Research Center 21000 Brookpark Road Cleveland, Ohio 44135	1
Mr. James E. Calkins Office of Research and Advanced Development NASA, Jet Propulsion Laboratory 4800 Oak Grove Drive Pasadena, California 91103	1
Mr. A. R. Raffaelli PR-2 NASA, John F. Kennedy Space Center Kennedy Space Center, Florida 32899	1

CENTERS (Cont'd)

Dr. A. H. Knothe Code TEC NASA, John F. Kennedy Space Center Kennedy Space Center, Florida 32899	1
Mr. Robert Hinckley NASA, Electronics Research Center Room 323 B 575 Main Street Cambridge, Massachusetts 02139	1
Dr. William G. Melbourne Mail Stop 180-300 Jet Propulsion Laboratory 4800 Oak Grove Drive Pasadena, California 91103	1
Scientific and Technical Information Facility Attn: NASA Rep. (S-AK/ RKT) P. O. Box 33 College Park, Maryland 20740	25
Mr. H. M. Drake, Chief Advanced Planning Office NASA, Flight Research Center Edwards Air Force Base Edwards, California 93523	1

DEPARTMENT OF DEFENSE

Dr. William W. Carter Chief Scientist U. S. Army Missile Command Bldg. 5250 Redstone Arsenal, Alabama	1
Mr. John McDaniel Technical Director Research and Development Directorate U. S. Army Missile Command Bldg. 4505 Redstone Arsenal, Alabama	12
Lt. M. V. Vasilik Arnold Air Force Base Tullahoma, Tennessee 37389	30

CONTRACTORS

The Boeing Company Attn: Mr. John Pehrson Huntsville Industrial Center Huntsville, Alabama	5
Brown Engineering Company, Inc. Mail Stop 5 300 Sparkman Drive, NW Huntsville, Alabama	5
Chrysler Corporation Attn: Mr. Howard Blood 1312 Meridian, North Huntsville, Alabama	5
Douglas Aircraft Holiday Office Center Huntsville, Alabama	5
General Electric Company Holiday Office Center Huntsville, Alabama	5
Mr. Robert A. Hardesty General Electric Company Ordnance Department 100 Plastics Avenue Room 1040 Pittsfield, Massachusetts 01201	5
Hayes International Corporation 204 Oakwood Avenue, NE Huntsville, Alabama	5
IBM Corporation 150 Sparkman Drive, NW Huntsville, Alabama	5
Lockheed Aircraft Corporation Holiday Office Center Huntsville, Alabama	5
North American Aviation, Inc. Holiday Office Center Huntsville, Alabama	5
Northrop Corporation Holiday Office Center Huntsville, Alabama	5
Mr. W. G. Calder General Electric Co. Suite 13 Holiday Office Center Huntsville, Alabama	1

CONTRACTORS (Cont'd)

Sperry Rand Corporation 8110 Memorial Parkway, SW Huntsville, Alabama	5
Space Craft, Incorporated 8620 Memorial Parkway, SW Huntsville, Alabama	1
Spaco, Incorporated 3022 University Drive, NW Huntsville, Alabama	5
University of Alabama 4701 University Avenue, NW Huntsville, Alabama	5
Vitro Corporation of America Holiday Office Center Huntsville, Alabama	5
Wyle Laboratories Highway 20, West Huntsville, Alabama	5
Mr. Robert Hardesty General Electric Company Ordinance Department 100 Plastics Avenue Room 1040 Pittsfield, Massachusetts 01201	1

UNIVERSITIES AND COLLEGES

Alabama A& M College Huntsville, Alabama	1
University of Alabama Tuscaloosa, Alabama	1
Dr. Clyde Hull Cantrell, Director Ralph Brown Draughon Library Auburn University Auburn, Alabama	4
University of California (UCLA) Los Angeles, California	1
Carnegie Institute of Technology Pittsburgh, Pennsylvania	1
Case Institute of Technology Cleveland, Ohio	1
Clemson University Clemson, South Carolina Attn: Mr. J. W. Gourlay	1

UNIVERSITIES AND COLLEGES (Cont'd)

Mr. S. G. Nicholas Director of Engineering Research Clemson University Clemson, South Carolina	1
Columbia University New York, New York 10027	1
Librarian Columbia University Nevis Laboratories Irvington, New York 10533	1
University of Denver Denver, Colorado	1
Director's Office Denver Research Institute University of Denver Denver, Colorado	1
Department of Nuclear Engineering Sciences University of Florida Gainesville, Florida 32603	1
Mrs J. Henley Crosland Director, Libraries Georgia Institute of Technology Atlanta, Georgia	9
University of Georgia Athens, Georgia	1
Louisiana State University Baton Rouge, Louisiana	1
Massachusetts Institute of Technology Cambridge, Massachusetts	1
University of Michigan Ann Arbor, Michigan	1
Mississippi State University State College, Mississippi	1
University of Mississippi University, Mississippi	1
University of North Carolina Chapel Hill, North Carolina	1

UNIVERSITIES AND COLLEGES (Cont'd)

Northeast Louisiana College Monroe, Louisiana	1
Ohio State University Columbus, Ohio	1
Ohio University Athens, Ohio	1
Oklahoma State University Stillwater, Oklahoma	1
University of Pittsburgh Pittsburgh, Pennsylvania	1
Princeton University Princeton, New Jersey	1
Library School of Electrical Engineering Purdue University Lafayette, Indiana	1
Rev. R. J. Henle, S. J. Vice President for Academic Matters and Research Director Saint Louis University 221 N. Grand Blvd. St. Louis, Missouri	2
Stanford University Palo Alto, California	1
Syracuse University Syracuse, New York	1
University of Tennessee Knoxville, Tennessee	1
Cushing Memorial Library Texas A& M University College Station, Texas	1
Mr. Harry E. Whitmore, Head Space Technology Division Texas A& M University College Station, Texas	2
University of Texas Austin, Texas	1

UNIVERSITIES AND COLLEGES (Cont'd)

Science Librarian Tulane University Library New Orleans, Louisiana 70118	1
The Joint University Libraries 419-21st Avenue, South Nashville, Tennessee	1
Science Library Vanderbilt University Box 1521, Station B Nashville, Tennessee	1
Virginia Polytechnic Institute Blacksburg, Virginia	1
Washington State Pullman, Washington	1
Mr. H. W. Hsu Associate Professor of Chemical Engineering University of Tennessee Knoxville, Tennessee 37916	1
Professor F. N. Peebles Department of Engineering Mechanics University of Tennessee Knoxville, Tennessee	1
Mr. W. Byron Long Director of Special Projects Mississippi Research and Development Center Jackson, Mississippi	1
Engineering Library University of Arkansas Fayetteville, Arkansas	1

UNITS OF MEASURE

In a prepared statement presented on August 5, 1965, to the U. S. House of Representatives Science and Astronautics Committee (chaired by George P. Miller of California), the position of the National Aeronautics and Space Administration on Units of Measure was stated by Dr. Alfred J. Eggers, Deputy Associate Administrator, Office of Advanced Research and Technology:

"In January of this year NASA directed that the international system of units should be considered the preferred system of units, and should be employed by the research centers as the primary system in all reports and publications of a technical nature, except where such use would reduce the usefulness of the report to the primary recipients. During the conversion period the use of customary units in parentheses following the SI units is permissible, but the parenthetical usage of conventional units will be discontinued as soon as it is judged that the normal users of the reports would not be particularly inconvenienced by the exclusive use of SI units."

The International System of Units (SI Units) has been adopted by the U. S. National Bureau of Standards (see NBS Technical News Bulletin, Vol. 48, No. 4, April 1964).

The International System of Units is defined in NASA SP-7012, "The International System of Units, Physical Constants, and Conversion Factors," which is available from the U. S. Government Printing Office, Washington, D. C. 20402.

SI Units are used preferentially in this series of research reports in accordance with NASA policy and following the practice of the National Bureau of Standards.